Lithos 294–295 (2017) 283–303

Contents lists available at ScienceDirect

Lithos

journal homepage: www.elsevier.com/locate/lithos

Reconstruction of multiple P-T-t stages from retrogressed mafic rocks: Subduction versus collision in the Southern Brasília orogen (SE Brazil)

Mahyra Tedeschi [a,b,c,*], Pierre Lanari [b], Daniela Rubatto [b,d], Antônio Pedrosa-Soares [a,1], Jörg Hermann [b], Ivo Dussin [a,e,1], Marco Aurélio P. Pinheiro [c], Anne-Sophie Bouvier [d], Lukas Baumgartner [d]

[a] Universidade Federal de Minas Gerais, Programa de Pos-Graduação em Geologia, CPMTC-IGC, Av. Antônio Carlos, 6627 Belo Horizonte, Brazil
[b] Institute of Geological Sciences, University of Bern, Baltzerstrasse1-3, Bern, Switzerland
[c] Geological Survey of Brazil (CPRM), Avenida Brasil, 1731 Belo Horizonte, MG, Brazil
[d] Institute of Earth Sciences, University of Lausanne, Geopolis, Lausanne, Switzerland
[e] Universidade do Estado do Rio de Janeiro, Multilab, Faculdade de Geologia, R. São Francisco Xavier, 524 Rio de Janeiro, Brazil

ARTICLE INFO

Article history:
Received 20 June 2017
Accepted 26 September 2017
Available online 10 October 2017

Keywords:
Petrochronology
Phase equilibrium
U-Th-Pb geochronology
Symplectite
XMapTools
Brasília orogen

ABSTRACT

The identification of markers of subduction zones in orogenic belts requires the estimation of paleo-geothermal gradients through pressure-temperature-time (P-T-t) estimates in mafic rocks that potentially derive from former oceanic units once. However, such markers are rare in supracrustal sequences specially in deeply eroded and weathered Precambrian orogens, and reconstructing their metamorphic history is challenging because they are commonly retrogressed and only preserve a few mineral relicts of high-pressure metamorphism. Metamorphosed mafic rocks from Pouso Alegre region of the Neoproterozoic Southern Brasília Orogen outcrop as rare lenses within continental gneisses. They have previously been classified as retrograde eclogites, based on the presence of garnet and the characteristic symplectitic texture replacing omphacite. These rocks were interpreted to mark the suture zone between the Paranapanema and São Francisco cratons. To test the possible record of eclogitic conditions in the Pouso Alegre mafic rocks, samples including the surrounding felsic rocks have been investigated using quantitative compositional mapping, forward thermodynamic modeling and in-situ dating of accessory minerals to refine their P-T-t history. In the metamorphosed mafic rocks, the peak pressure assemblage of garnet and omphacite (Jd_{20}, reconstructed composition) formed at 690 ± 35 °C and 13.5 ± 3.0 kbar, whereas local retrogression into symplectite or corona occurred at 595 ± 25 °C and 4.8 ± 1.5 kbar. The two reactions were coupled and thus took place at the same time. A zircon U-Pb age of 603 ± 7 Ma was obtained for metamorphic rims and linked to the retrogression stage. Monazite and metamorphic zircon U-Th-Pb ages for the surrounding rocks are at ca. 630 Ma and linked to peak pressure conditions similar to the one recorded by the mafic rocks. The low maximal pressure of 14 kbar and the high geothermal gradient do not necessarily support subduction process-related metamorphism but, more likely, metamorphism related to continental collision.
© 2017 Elsevier B.V. All rights reserved.

1. Introduction

Mafic rocks within collisional orogens may be used as markers for oceanic subduction zones, particularly if they preserve relicts of eclogite facies metamorphism (Evans et al., 1979; Ganade de Araujo et al., 2014; Gilotti, 2013; Heinrich, 1986; Singh et al., 2013; Weller and St-Onge, 2017). Lenses of mafic rocks metamorphosed at high-pressure (HP) within felsic crustal sequences that lack evidence for HP metamorphism are common in numerous orogenic belts from the Paleoproterozoic (e.g. Belemorian province, Liu et al., 2017; Trans-Hudson orogeny, Weller and St-Onge, 2017) to the Cenozoic (e.g. Tso Morari in Himalaya, Guillot et al., 2007; Adula Nappe in the Alps, Heinrich, 1986). Relict HP (20–30 kbar) mineral assemblages in such mafic boudins have been attributed to subduction-related metamorphic processes and thus used as markers of suture zones. However, the P-T trajectories of such rocks should be carefully determined in order to indicate in which geodynamic scenario (subduction or collision) they have formed. This is particularly important for rocks whose P-T conditions are located below the coesite stability field and thus cannot be directly related to subduction (Brown, 2009). Because such rocks play an important role in informing geodynamic models (Godard, 2001; McClelland and Lapen, 2013) determining the correct, maximal P-T conditions they reached is crucial.

Reconstructing the pressure-temperature-time (P-T-t) history of polymetamorphic mafic rocks within felsic units is challenging. Firstly,

* Corresponding author at: Universidade Federal de Minas Gerais, Programa de Pos-Graduação em Geologia, CPMTC-IGC, Av. Antônio Carlos, 6627 Belo Horizonte, Brazil.
E-mail address: mahyra.tedeschi@cprm.gov.br (M. Tedeschi).
[1] Fellow of the Brazilian Research Council-CNPq.

https://doi.org/10.1016/j.lithos.2017.09.025
0024-4937/© 2017 Elsevier B.V. All rights reserved.

mafic lenses are scarce in deeply eroded terranes rich in orthogneisses and paragneisses, where they are commonly retrogressed because of late amphibolite to granulite facies metamorphism and/or strong interaction with fluids during exhumation (Lanari et al., 2013). Thermobarometric investigations are complicated as only a few relicts of the HP mineral assemblage are preserved. In Precambrian belts, it can be even more difficult to recognize high-pressure relicts because of long lasting surface weathering.

Metamorphosed mafic rocks from Pouso Alegre in the Neoproterozoic Southern Brasília orogen, in SW-Brazil (Fig. 1A; Campos Neto and Caby, 1999; Coelho et al., 2017; Trouw et al., 2013) are a typical example of such complex rocks. They crop out as scarce lenses within migmatitic sillimanite-garnet gneiss, migmatitic amphibole-garnet orthogneiss, biotite gneiss, granite and mafic rocks (Fig. 1C). They have been previously classified as "retro-eclogites" (Choudhuri et al., 1978; Hoppe et al., 1985; Trouw et al., 2013), based on the presence of garnet, considered as the only remnant of the HP assemblage, (assumed omphacite + garnet, Coelho et al., 2017) and typical retrogression products such as symplectite and coronitic textures. However, no quantitative estimate of the peak pressure is available to support this interpretation. Nevertheless, these metamorphosed mafic rocks have been quoted as markers of a suture zone formed after oceanic subduction between the Paranapanema

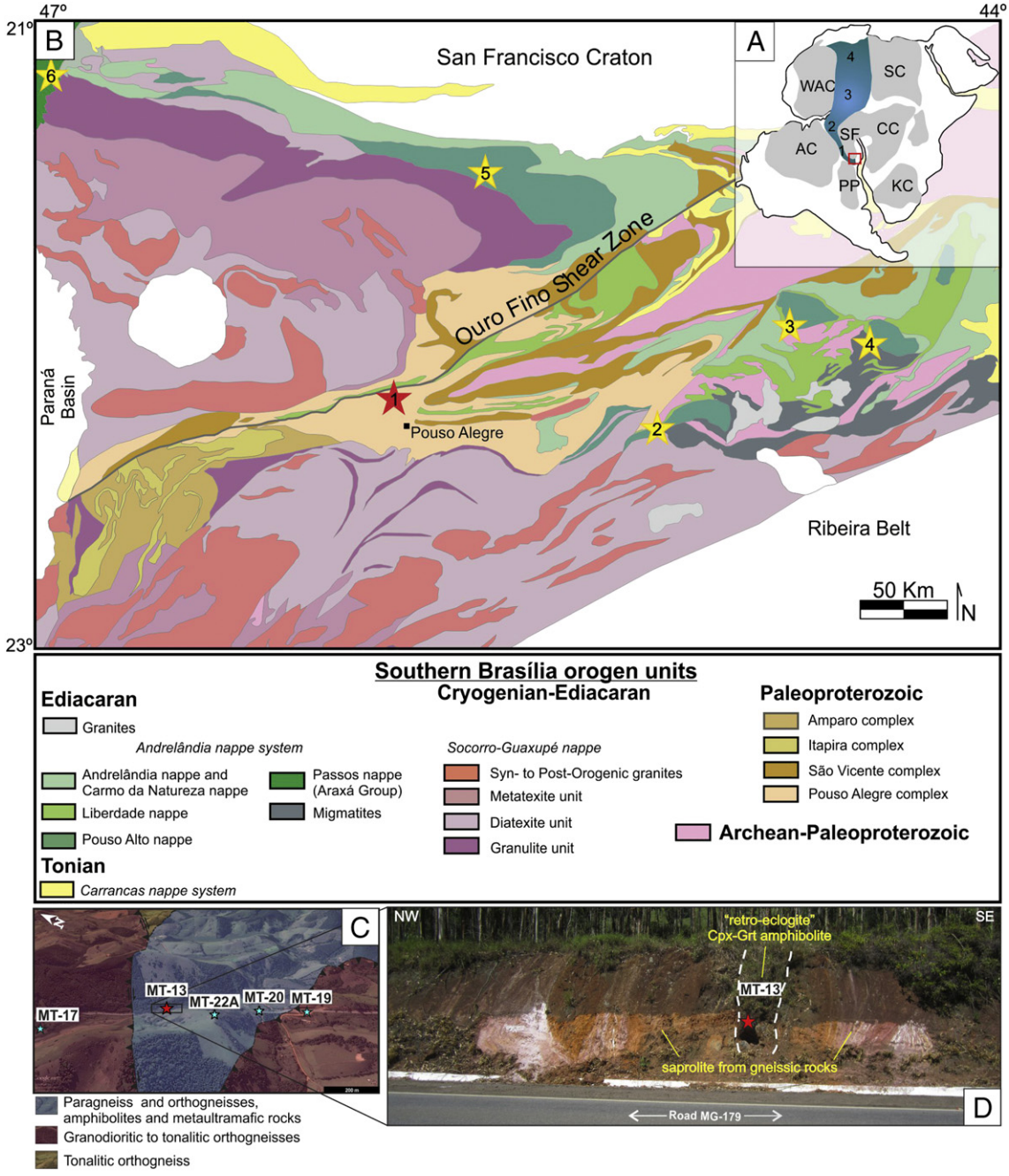

Fig. 1. (A) Distribution of cratonic blocks and orogenic belts in Western Gondwana (red rectangle: location of the studied region illustrated in B): WAC, West African craton; SC, Sahara meta-craton; AC, Amazonian craton; SF, São Francisco craton; CC, Congo craton; PP, Paranapanema block; KC, Kahalari craton; West Gondwana orogen (in blue), including the Brasília orogen (1), Borborema province (2), Dahomide (3) and Oubanguide (4) belts (modified from De Wit et al., 2008; Ganade de Araujo, 2014). (B) Sketch map of the Southern Brasília orogen (modified from Campos Neto et al., 2011; Westin et al., 2016). Red star (1): location of the studied "retro-eclogite" occurrence of Pouso Alegre. Yellow stars: other occurrences of "retro-eclogites" (2-Varginha nappe, 3-Airuoca klippe, 4- Liberdade nappe, 5-Carmo do Cachoeira nappe and 6-São Sebastião do Paraíso). (C) Location of the studied samples in the geological map (Ribeiro et al., 2011) on the terrain image (Google Earth®). (D) Outcrop photo showing the clinopyroxene-garnet amphibolite flanked by saprolites of gneisses. (For interpretation of the references to colour in this figure legend, the reader is referred to the web version of this article.)

and São Francisco cratons (Campos Neto et al., 2011; Coelho et al., 2017; Trouw et al., 2013).

Since reconstructing the metamorphic pressure-temperature-time evolution of retrogressed mafic samples is challenging, it requires a detailed petrochronological approach. It is necessary to clearly identify the mineral relicts formed during the HP stages, and to analyze their chemical and isotopic compositions. It has been shown that the use of quantitative compositional mapping (Lanari et al., 2013; Loury et al., 2016) and the study of mineral inclusions in accessory minerals (Hart et al., 2016; Hermann et al., 2001) are efficient techniques to identify HP relicts that are no longer preserved in the mineral matrix and to reconstruct P-T-t conditions. Thermobarometric estimates can be obtained from thermodynamic forward models such as equilibrium phase diagrams (e.g. Powell and Holland, 2008) and this technique can be enhanced by restricting the investigations to local domains, i.e., to retrieve the physical and chemical conditions (P-T-X) of a specific reaction (Lanari and Engi, 2017, and references therein). Accessory phases can be dated and linked to the growth or breakdown of major phases to constrain specific P-T-t stages (e.g., Rubatto and Hermann, 2001).

In this study, we combine quantitative compositional mapping (Lanari et al., 2012, 2014), with forward thermodynamics modeling to retrieve the maximal P conditions recorded by a mafic rock of Pouso Alegre. A comprehensive approach, that uses the local density corrected composition of the symplectite domain and compares it to the omphacite composition obtained by the model, was applied to retrieve the former omphacite composition. Subsequent retrogression stages are examined from modeling local domains and their chemical and chronological relationships are evaluated by mass balance (Centrella et al., 2015). U-Th-Pb ages from zircon and monazite provide time constraints for two distinct metamorphic events. They are correlated to P-T estimates using inclusion compositions, trace elements on zircon, monazite, garnet and rutile, with Zr-in-rutile and Ti-in-zircon thermometry. The evolution of the mafic rock is related to that of the country rocks for which additional P-T estimates, as well as zircon and monazite ages were obtained. Appendix A presents the descriptions of the analytical methods applied in the following sections.

2. Geological setting

The Brasília orogenic system is a 1800 km-long, nearly N-S trending belt, extending roughly between the 10° and 26° S parallels. It is one of the orogenic belts formed during West Gondwana amalgamation in Neoproterozoic time (Cordani et al., 2003; Fig. 1A). The northern and southern segments of that orogenic system evolved separately in relation to distinct paleocontinental blocks (Fuck et al., 2017; Valeriano, 2017). The Southern Brasília belt has been related to the convergence of the Paranapanema and São Francisco paleocontinental blocks (Fig. 1B), involving oceanic subduction and collisional orogeny, which resulted in stacked nappe systems verging to east (Campos Neto et al., 2011; Mantovani and Brito-Neves, 2005; Trouw et al., 2000, 2013).

Each nappe system represents a specific compartment with distinctive tectono-metamorphic features (Fig. 1B). The Socorro-Guaxupé nappe (SGN) is mainly composed of meta-igneous rocks from a Neoproterozoic magmatic arc, with minor paragneisses and schists (Campos Neto and Caby, 2000; Rocha et al., 2016), and is placed over the metasedimentary rocks of the Andrelândia nappe system (ANS). Those ANS metasedimentary rocks show an inverted metamorphic pattern, with high-pressure granulite and eclogite facies on top, and amphibolite to greenschist facies at the base (Campos Neto et al., 2011; Trouw et al., 2013). Studies on ANS described mixtures of sediments derived from both active and passive margins (Belém et al., 2011; Trouw et al., 2013). Campos Neto et al. (2011) suggested that they represent subduction-related metasedimentary sequences, forming an accretionary prism. The continental margin of the lower plate is then related to São Francisco Craton and represented by the Carrancas nappe system (Fig. 1B; Campos Neto et al., 2011; Trouw et al., 2000). Depending on the interpretation, the suture zone is located above (Trouw et al., 2013) or below the ANS (Campos Neto et al., 2011).

The investigated samples are from the tectonic boundary between the SGN and ANS, located 20 km to the northeast of Pouso Alegre city, along the Ouro Fino shear zone (Table 1; Fig. 1B and C). This shear zone is 300 km long and cuts a wide tectonic window disclosing Archean and Paleoproterozoic migmatitic orthogneisses of the Pouso Alegre complex (Cioffi et al., 2016). It has been interpreted as the reworked margin of the São Francisco Craton, tectonically interleaved with orthogneisses and metasedimentary rocks of the SGN and ANS (Ribeiro et al., 2011).

The recently proposed Neoproterozoic West Gondwana orogen (WGO; Ganade de Araujo et al., 2014) is a roughly linear belt that extended for more than 4000 km from the present-day Northeast Africa to Central Brazil (Fig. 1A). The reconstruction of this paleo-subduction zone was mostly based on chrono-correlations of HP to UHP rocks from Mali, Togo and NE-Brazil. As one of the oldest known deep continental subduction zones in geological history, the existence of this long suture has implications for life sustainability in the Ediacaran (Ganade de Araujo et al., 2014) and for the geotectonic evolution of Central Brazil. The extension of this suture further to the south is solely based on the possible presence of HP rocks of Ediacaran age in the Southern Brasília orogen (Campos Neto et al., 2011; Campos Neto and Caby, 1999, 2000; Parkinson et al., 2001; Trouw et al., 2000, 2013). Such HP rocks are mainly garnet amphibolites, with plagioclase being interpreted as retrograde, labeled as "retro-eclogites" (e.g., Choudhuri et al., 1978; Hoppe et al., 1985). They are found in several places, like Pouso Alegre, Liberdade, Varginha and Passos (São Sebastião do Paraíso) nappes (Fig. 1B).

Those "retro-eclogites" were firstly classified by Choudhuri et al. (1978), after studies on rocks from the Pouso Alegre region that show the garnet + clinopyroxene assemblage in the presence of symplectite and corona. Coelho et al. (2017) determined metamorphic conditions of 12 to 16 kbar at 700 to 800 °C for the same rocks, suggesting that the higher pressure assemblages were completely overprinted. Hoppe et al. (1985) reported that the eclogitic rocks from northern Pouso Alegre (PA) and São Sebastião do Paraíso (SSP) contain symplectites and coronitic textures only at PA, where migmatitic paragneisses and orthogneisses constitute the associated rocks. Using the composition of pyroxene (Jd_{30} from SSP, but not PA) Hoppe et al. (1985) estimated 630 °C and 7–8 kbar as minimum conditions for the eclogite and 490 ± 50 °C for the retrograde stage corresponding to amphibole formation. Campos Neto and Caby (1999) indicated maximum pressures of 17.5 kbar (for a $T = 660$ °C) in the Liberdade nappe, located northeast of Pouso Alegre. Parkinson et al. (2001) described coesite as inclusion in zircon hosted by kyanite-garnet-hypersthene granulites from the Varginha nappe in the NW of Pouso Alegre, but no spectroscopy details were provided to support this finding. Trouw (2008) proposed that rocks from Virgínia, to the SE of Pouso Alegre, reached eclogitic facies based on their clinopyroxene-garnet composition and plagioclase corona.

3. Sample description

Five samples were collected along a 2 km NW-SE transect at 20 km to the northeast of Pouso Alegre (Road MG-179; Fig. 1B and C). The main rock for this study, the clinopyroxene-garnet amphibolite (sample MT-13), crops out as a meter-thick lens of fresh metamorphic mafic rock enveloped by a steep-dipping assemblage of saprolitic to well-preserved rocks (Fig. 1D). Samples from the host rocks are a migmatitic amphibole-garnet gneiss with augen structure (MT-17), a deformed allanite-bearing biotite granite (MT-19), and a biotite gneiss (MT-20). By comparison with the country rocks in the region, the host rocks of the mafic lens can be correlated to the Pouso Alegre Complex (Cioffi et al., 2016). Interleaved migmatitic sillimanite-garnet gneiss (MT-22A) shows sharp to mylonitic contact with the aforementioned

Table 1
Summary details for the Pouso Alegre samples. UTM coordinates are relative to the WGS84 datum.

Sample	Lithology	UTM coordinates		Mineral assemblage		Protolith age (Ma)		Metamorphism age (Ma)		P-T conditions	
		E	N	Major	Minor/Aces.	LA-ICP-MS	+SIMS	LA-ICP-MS	+SIMS	T (°C)	P (kbar)
MT-13	Grt-Cpx amphibolite	409,623	7,560,455	Grt + Cpx + Amp + Pl + Qz	Rt + Ilm + Ttn + Zrn	–	1513 ± 17		603 ± 7	720 ± 30	13.4 ± 2.8
MT-17	migmatitic Grt-Amp gneiss	408,216	7,561,674	Grt + Amp + Pl + Kfs + Bt + Qz	Ep + Ttn + Zrn	2066 ± 2	–	–	–	~700	~14
MT-19	Aln-bearing Bt granite	409,525	7,560,729	Bt + Pl + Kfs + Qz	Aln + Zrn	2076 ± 3	–	626 ± 5	–	–	–
MT-20	Bt gneiss	408,714	7,560,425	Bt + Pl + Kfs + Qz	Grt + Zrn	2076 ± 4	–	632 ± 2	–	–	–
MT-22A	migmatitic Sil-Grt gneiss	409,473	7,560,974	Sil + Grt + Kfs + Ms. + Qz + Bt	Mnz + Zrn	794 ± 4	–	672 ± 4 (Zrn)	637 ± 7 (Mnz)	–	–

rocks. After field mapping, the migmatitic sillimanite-garnet gneiss was correlated to the Andrelândia Group, a unit mapped in the area (Ribeiro et al., 2011; Fig. 1C). The clinopyroxene-garnet amphibolite is better preserved in its inner part, where it is weakly to non-foliated, while at the borders it shows a mylonitic foliation. The country rocks show the same steep-dipping tectonic foliation imprinted in the lens of clinopyroxene-garnet amphibolite, corresponding to the mylonitic foliation related to the Ouro Fino shear zone.

3.1. Petrography

The clinopyroxene-garnet amphibolite MT-13 comes from an inner and less deformed portion of the mafic lens. This sample contains mm- to cm-sized pinkish poikiloblastic garnet. Each crystal exhibits an irregular shape with lobate edges (Fig. 2A and B) being systematically surrounded by a composite corona made of inner plagioclase and outer amphibole. Garnet in contact with clinopyroxene is rare. The garnet porphyroblasts show several inclusions, including rutile, zircon, clinopyroxene and quartz. Clinopyroxene in contact with amphibole forms subhedral crystals, or is developed within a symplectite, together with plagioclase, amphibole and quartz (Figs. 2A and B, 3). Ilmenite, rutile, apatite, zircon and titanite are minor phases in this sample. Rutile grains are present as inclusions in garnet, amphibole, clinopyroxene (symplectite and subeuhedral crystals) and in the plagioclase corona. As well as ilmenite, rutile is often surrounded by a titanite corona. Twenty per cent of rutile crystals (530 have been investigated) contain inclusions of zircon and ilmenite, and only 4% have silicate inclusions such as clinopyroxene, amphibole, garnet, feldspar, quartz, titanite and biotite (Supplementary Fig. S.1). SiO_2 inclusions were checked by Raman spectroscopy and they all resulted made of quartz and no higher pressure polymorphs were found.

The felsic and intermediate country rocks include a migmatitic gneiss (samples MT-17, Fig. 2E and F), a granite (MT-19), an orthogneiss (MT-20) and a migmatitic sillimanite-garnet gneiss (sample MT-22A, Fig. 2C and D). Sample MT-22A is a greyish, fine-grained stromatic gneiss exhibiting millimetric bands of leucosome and melanosome (Fig. 2C). The leucosome bands are composed of K-feldspar and quartz ribbons, while the melanosome bands consist of fibrous sillimanite (mostly replaced by white mica), feldspar (highly weathered to clay minerals) and millimetric red garnet porphyroblasts. Garnet crystals, exhibiting a pseudo-automorphic shape with only few lobate edges, have quartz inclusions and are locally replaced by biotite, which also grew in rotated pressure shadows (Fig. 2D). Owing to the weathering alteration, it is impossible to determine the original bulk chemical composition of sample MT-22A.

Sample MT-17 (Fig. 2E) is a stromatic amphibole-garnet gneiss, showing alternating melanocratic and leucocratic bands, and augen structure. The melanosome consists of millimetric red garnet, dark-green amphibole, biotite and oligoclase. The leucosome consists of medium- to coarse-grained oligoclase, microcline and quartz (Fig. 2F). Titanite, ilmenite, epidote, zircon and apatite are accessory phases. The melanocratic bands show clusters of titanite and epidote. Sample MT-19 is a deformed, fine-grained allanite-bearing biotite metagranite. Allanite and zircon are the minor phases. Sample MT-20 is a biotite orthogneiss with minor garnet (1–2 vol%), showing incipient mylonitization, with millimetric plagioclase and quartz porphyroclasts surrounded by biotite. White mica locally replaces biotite. Zircon and apatite are accessory phases.

3.2. Petrographic interpretation

The clinopyroxene-garnet amphibolite MT-13 is highly retrogressed as shown by the presence of symplectite, corona and titanite overgrowth over rutile. The symplectite observed in this sample is typical of retrogressed mafic eclogites and formed through the reaction omphacite + H_2O → clinopyroxene + plagioclase + amphibole ± quartz (Lanari et al., 2013; Waters, 2003). The general shape of garnet crystals showing lobate edges suggests garnet resorption (Lanari et al., 2017; Robyr et al., 2014) that may have occurred during the formation of the corona. Plagioclase and amphibole systematically appear in sequence of zones in the corona around garnet (Fig. 3). Chemical potential gradients are interpreted to control the mineral sequence observed in the corona (Carlson and Johnson, 1991; White et al., 2008). The spatial distribution of minerals is thus due to limited intergranular diffusion of some species, such as Al_2O_3. Rutile is interpreted to have formed early during the metamorphic history, as it has been trapped as inclusion by most of the major phases.

Both the migmatitic sillimanite-garnet gneiss MT-22A and the migmatitic amphibole-garnet gneiss MT-17 can be interpreted as highly deformed stromatic migmatites, since microcline and quartz make up the major part of the felsic layers. Features like discordant leucosome veins, schöllen and schlieren textures, which can be evidence of melt migration (cf. Sawyer, 2008), are absent. The distribution of the weathering products (clay-minerals) and the preservation of twinning suggest that former plagioclase has been strongly weathered in sample MT-22A. The idiomorphic shape of the garnet crystals suggests little or no resorption. In MT-17, secondary biotite locally replaces amphibole and garnet. The fine-grained allanite-bearing biotite granite (MT-19) and biotite gneiss (MT-20) are closely located to each other and have similar mineralogical composition.

4. Results

4.1. Bulk rock chemistry

Bulk rock chemistry data are available in Supplementary Data 1 and the diagrams in Supplementary Fig. S.2.

Clinopyroxene-garnet amphibolite MT-13 has a basaltic composition with tholeiitic affinity. Chondrite-normalized trace element spider and REE diagrams show a pattern between N-MORB and *E*-MORB.

Amphibole-garnet migmatitic gneiss MT-17 shows a composition between diorite and granodiorite (SiO_2 = 62.5 wt%). It exhibits the highest enrichment in REE among the sample set, with $(La/Sm)_N$ = 3.0 and $(Tb/Yb)_N$ = 1.66 and an approximately flat distribution for the

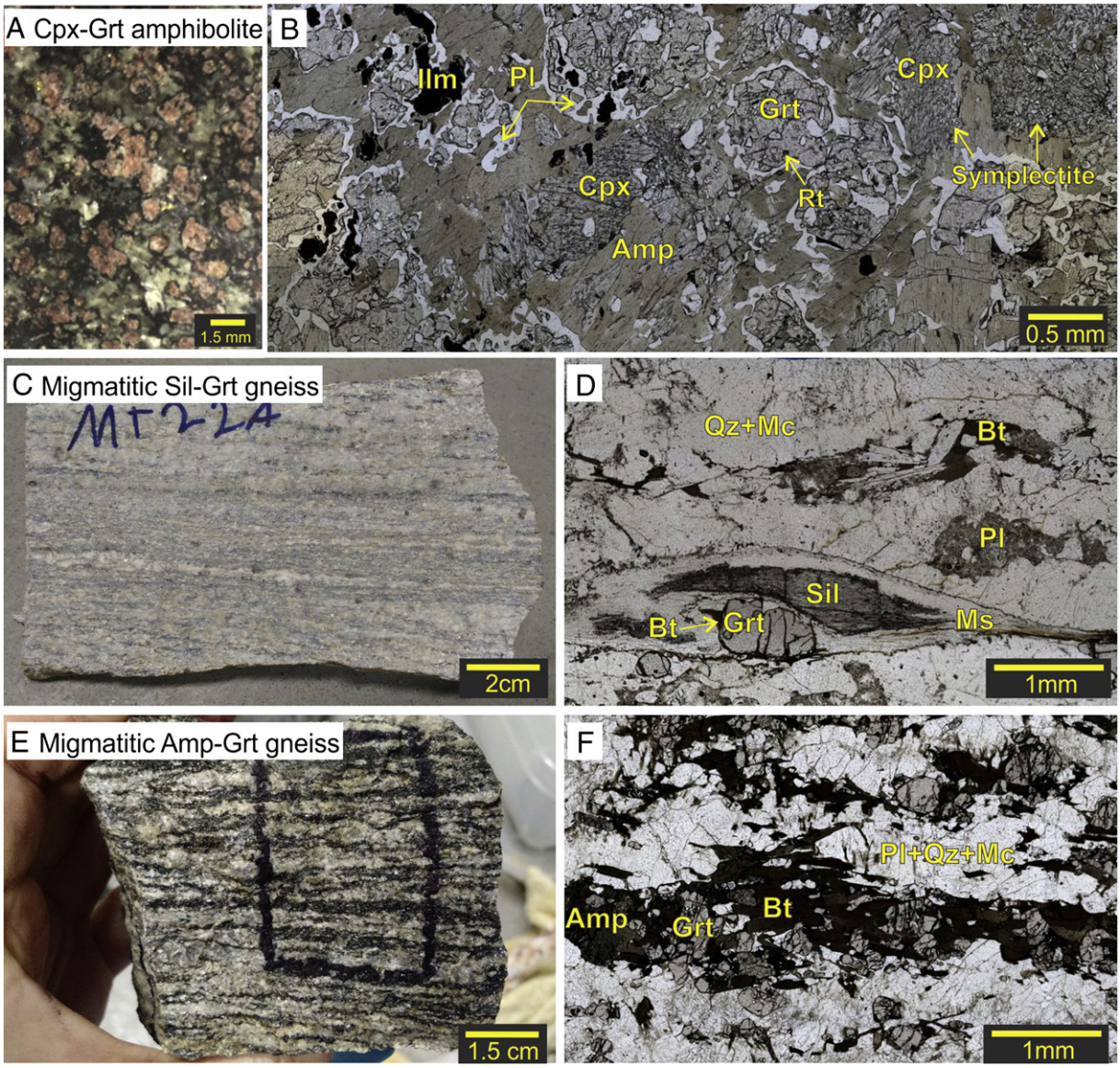

Fig. 2. Hand specimen and transmitted light photomicrographs of: (A–B) clinopyroxene-garnet amphibolite MT-13, (C–D) migmatitic sillimanite-garnet gneiss MT-22A, with the yellow narrow indicating the biotite rotated shadow, and (E–F) migmatitic amphibole-garnet augen gneiss MT-17. (For interpretation of the references to colour in this figure legend, the reader is referred to the web version of this article.)

HREE. Both the allanite-bearing biotite granite MT-19 and biotite gneiss MT-20 are calc-alkaline, with granitic and granodioritic compositions, respectively. The first exhibits high LREE contents and $(La/Sm)_N = 5$, with a slight negative slope for the HREE distribution with $(Tb/Yb)_N = 2.9$ and a positive Eu anomaly ($Eu/Eu^* = 1.3$). The positive Eu anomaly suggests accumulation of plagioclase. Sample MT-20 shows enrichment in LREE and $(La/Sm)_N = 4.27$, but is extremely depleted in HREE with $(Tb/Yb)_N = 1.96$, and shows a negative Eu anomaly ($Eu/Eu^* = 0.52$). The spider diagram shows negative anomalies for P and Ti for samples MT-17, MT-19 and MT-20 and of Nb for sample MT-19.

4.2. Mineral compositions

X-ray compositional maps were acquired by electron probe microanalyser (EPMA) and standardized in concentration maps of oxide weight percentage using the internal standard technique (De Andrade et al., 2006) and the program XMapTools 2.3.1 (Lanari et al., 2014). Structural formula maps in atom per formula unit (apfu) were used to investigate the compositional variability of the mineral phases at the thin section scale. Representative mineral compositions are available in the Supplementary Data files 2 (MT-13), 3(MT-22A) and 4(MT-17), and the compositional maps in Supplementary Figs. S.3, S.4, S.5 and S.6.

Garnet in clinopyroxene-garnet amphibolite MT-13 shows a relatively homogeneous chemical composition for the core of the grains (Figs. 3C and S.3) with an average structural formula of $Alm_{53}Prp_{19}Grs_{26}Sps_{1.5}$. Slight compositional zoning is observed within this core, especially in Ca ($Grs_{24–28}$) and Fe ($Alm_{51–54}$). A thin rim of ~25 μm thickness systematically occurs at the contact with the corona. The average structural formula of the rim is $Alm_{58}Prp_{18}Grs_{22}Sps_{2.3}$. Mn-content increases from 0.05 apfu in the core to 0.07 apfu in the near-rim zone.

Similarly to garnet, clinopyroxene in sample MT-13 shows slight compositional variations between the grains located in different domains (Figs. 4 and S.4). Clinopyroxene has low Na-content ($Jd_{3–5}$) and XMg ($Mg^{2+} / (Mg^{2+} + Fe^{2+})$) ranging from 0.70 to 0.74. The highest jadeite content (Jd_5) is observed in grains located in both garnet and symplectite. It is important to note that some of the clinopyroxene grains present as "pseudo-inclusions" in garnet could also be linked to the corona or to an early symplectite stage and appear as "inclusions" because of 3D sectioning effects. As the clinopyroxene composition

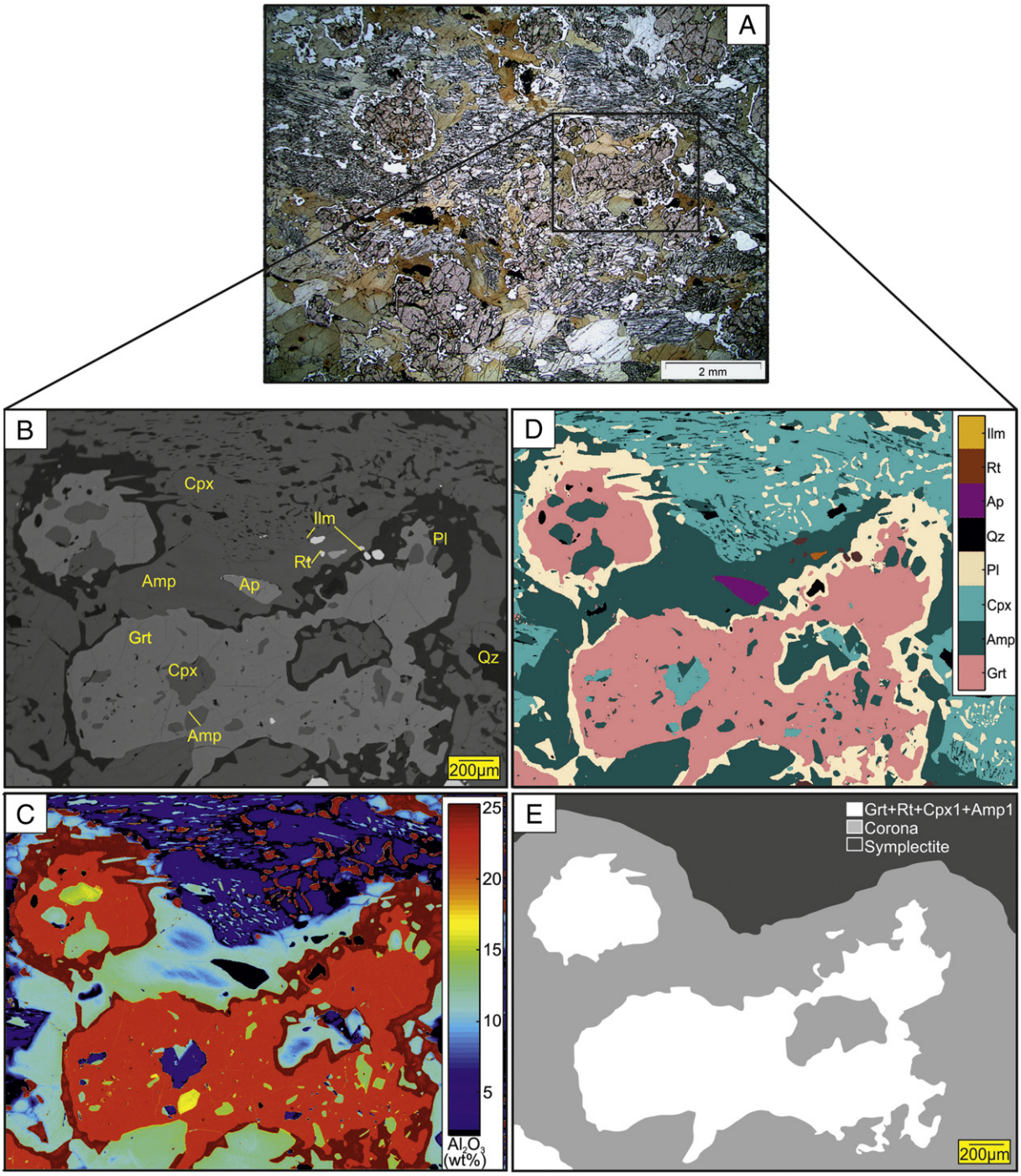

Fig. 3. Photomicrograph (A) showing the texture of clinopyroxene-garnet amphibolite MT-13 with the selected rectangle area mapped showed in: (B) Backscattered image; (C) Al_2O_3 (wt%) compositional map from XMapTools; (D) Phases maps and (E) Distinct assemblages identified from texture and compositional map.

does not significantly change between the different domains, it is labeled Cpx2 and related to the growth of the corona and symplectite. No relict of HP clinopyroxene (Cpx1) with omphacite composition is preserved in the investigated domain. Several spot analyses of clinopyroxene inclusions in garnet, rutile and garnet were measured and the highest jadeite content observed is Jd_8.

Amphibole in sample MT-13 has a composition varying from ferroan-hornblende to hornblende (cf. Tindle and Webb, 1994). Amphibole occurs as: (a) coarse grains in the corona, (b) fine grains in the symplectite and (c) inclusions in garnet. (a) The coarse-grained amphibole surrounding the plagioclase in the corona is compositionally zoned, with a core depleted in Al (1.4 apfu), Na (0.4 apfu), Ca (1.74 apfu) and high XMg (0.64). The chemical zoning of the amphibole rim is asymmetric with slightly different compositions observed in the direction of garnet (Al = 2.3 apfu; Na = 0.6 apfu, Ca = 1.84 apfu; XMg = 0.58) or toward the symplectite (Al = 1.7 apfu; Na = 0.55 apfu, Ca = 1.84 apfu; XMg = 0.62). (b) The fine-grained amphibole in the symplectite shows similar composition to the amphibole in the outer part of the corona, located close to the symplectite. (c) Amphibole inclusions in garnet show variable chemical compositions. Those associated to plagioclase show the same composition/zoning pattern as those from the outer-garnet corona (Figs. 4 and S.5). Other inclusions are more homogeneous in composition with higher Al (2.5–3.0 apfu), Na (0.65 apfu), Ca (1.86 apfu)), and lower XMg (0.50–0.55). Plagioclase

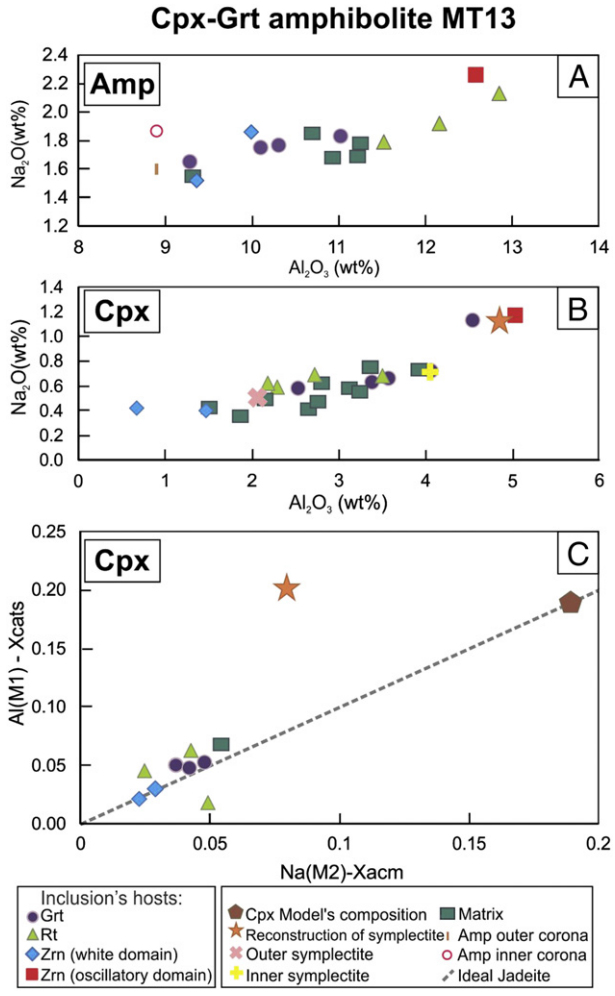

Fig. 4. Na_2O vs Al_2O_3 diagram for amphibole (A) and clinopyroxene (B) compositions from the clinopyroxene-garnet amphibolite (MT-13). (C) Al (M1)-Xcats vs Na (M2)-Xacm diagram with the distribution of stoichiometric clinopyroxene compositions, Jadeite ideal composition and reconstructed symplectite composition (see text for details).

is present in the corona and in the symplectite (Fig. 3). In the corona, plagioclase composition varies from An_{40} at the contact with garnet to An_{35-28} at the contact with amphibole. In the symplectite, plagioclase shows homogeneous composition of An_{27}.

Garnet poikiloblasts in the migmatitic sillimanite-garnet gneiss MT-22A show compositional zoning features similar to MT-13 (Fig. S.6) with an increase of Fe and Mn from core ($Alm_{82}Prp_{8.5}Grs_6Sps_1$) to rim ($Alm_{85}Prp_{6.5}Grs_4Sps_4$). From the zoning pattern, it appears that several small crystals constitute each poikiloblast. There is no apparent change in garnet composition associated to fractures or inclusions. EPMA spot analyses were also performed on the weathered phase that constitutes around 15 vol% of the rock. The results show a low oxide weight percentage sum (74–80 wt%), explained by the presence of clay minerals. The augen gneiss MT-17 exhibits almandine-rich garnet with an average composition of $Alm_{60-67}Grs_{27-33}Prp_{2-5}Sps_{1-3}$. Amphibole from its mafic bands constitutes potassium pargasite to potassium hornblende compositions (XMg = 0.19–0.22).

4.3. Thermobarometry

4.3.1. Phase equilibria

In order to reconstruct the P-T evolution of sample MT-13, isochemical phase diagrams were produced for different bulk compositions using Theriak-Domino (de Capitani and Brown, 1987; de Capitani and Petrakakis, 2010), the internally consistent thermodynamic dataset TC55 (Holland and Powell, 1998 and subsequent updates), together with the following solid solution models: garnet (Holland and Powell, 1998); clinopyroxene (Holland and Powell, 1996); amphibole (Diener et al., 2007); plagioclase (Baldwin et al., 2005); and an ideal model for ilmenite. The chemical system was simplified to Na_2O–CaO–FeO–MgO–Al_2O_3–SiO_2–H_2O–TiO_2 because of the absence of K- and Mn-bearing phases. Whereas the presence of Mn in the model affects the size of the stability field of garnet (Tinkham et al., 2001), the effect on the position of garnet isopleths is limited for low-spessartine contents garnets (<2%) as those observed in this sample. The computations were carried out assuming a saturating pure H_2O fluid ($a_{H2O} = 1$). Due to the presence of ilmenite, Fe is assumed to be all Fe^{+2}. The program GrtMod (Lanari et al., 2017), which applies an automated strategy to minimize an objective function that represents the difference between the observed and modelled garnet composition, was used for the determination of the optimal P-T conditions from garnet composition.

In the clinopyroxene-garnet amphibolite, at least two metamorphic stages have been identified and defined by different phases: i) garnet and rutile for the prograde to HP stage (Fig. 5); ii) symplectite and corona for the retrogression (Fig. 6). Owing to the strong retrogression, only few relics of the HP stage are observed and the HP assemblage is unknown. As no weathering is observed in this sample, the unmodified bulk rock composition was used to model the stable assemblage, mineral phase proportions and compositions conditions of the HP stage. This assumption strongly relies on the preservation of the original bulk rock composition in a closed system and on the absence of significant compositional changes during retrogression (this hypothesis is tested in Section 5.1.2).

According to the P-T isochemical phase diagram for the bulk rock composition of sample MT-13 (Fig. 5), optimal P-T conditions of

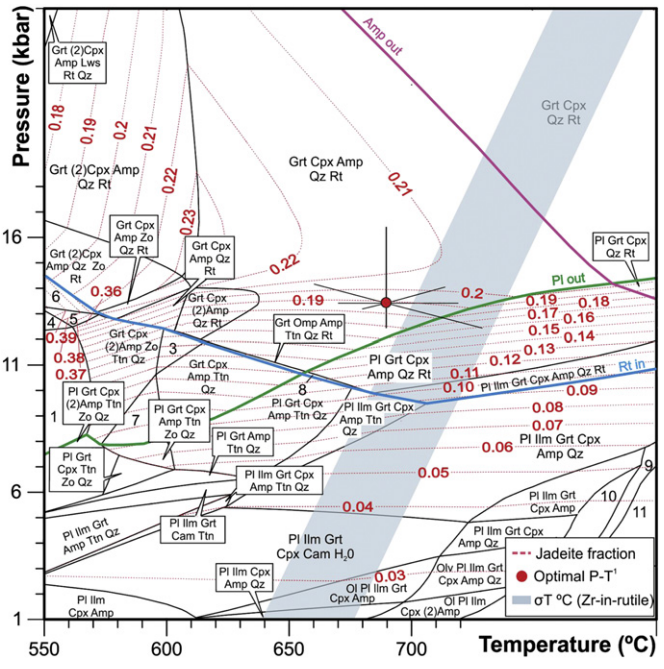

Fig. 5. Pressure-temperature (P-T) diagram calculated with Theriak-Domino (de Capitani and Petrakakis, 2010) showing the estimated P-T conditions for the clinopyroxene-garnet amphibolite MT-13 obtained with (1) GrtMod (Lanari et al., 2017) and in accordance with the Jd fraction estimated from the reconstruction of the symplectite (Section 5.1.1). Zr-in-rutile thermometry with 1σ results are shown in the blue field. Numbers for the fields: 1-Grt (2)Amp Zo Ttn Qz, 2-Grt Omp (2)Amp Zo Ttn Qz, 3-Grt Omp (2)Amp Ttn Qz 4-Grt Amp Zo Ttn Qz, 5-Grt Omp Amp Zo Ttn Qz, 6-Grt Omp Amp Zo Ttn Qz, 7-Grt Omp Amp Zo Ttn Qz, 8-Fsp Grt Omp Amp Ttn Qz Rt, 9-Fsp Ilm Grt Omp Opx Amp Qz, 10-Fsp Ilm Grt Omp Amp Qz and 11-Fsp Ilm Grt Omp Opx (2)Amp Qz. (For interpretation of the references to colour in this figure legend, the reader is referred to the web version of this article.)

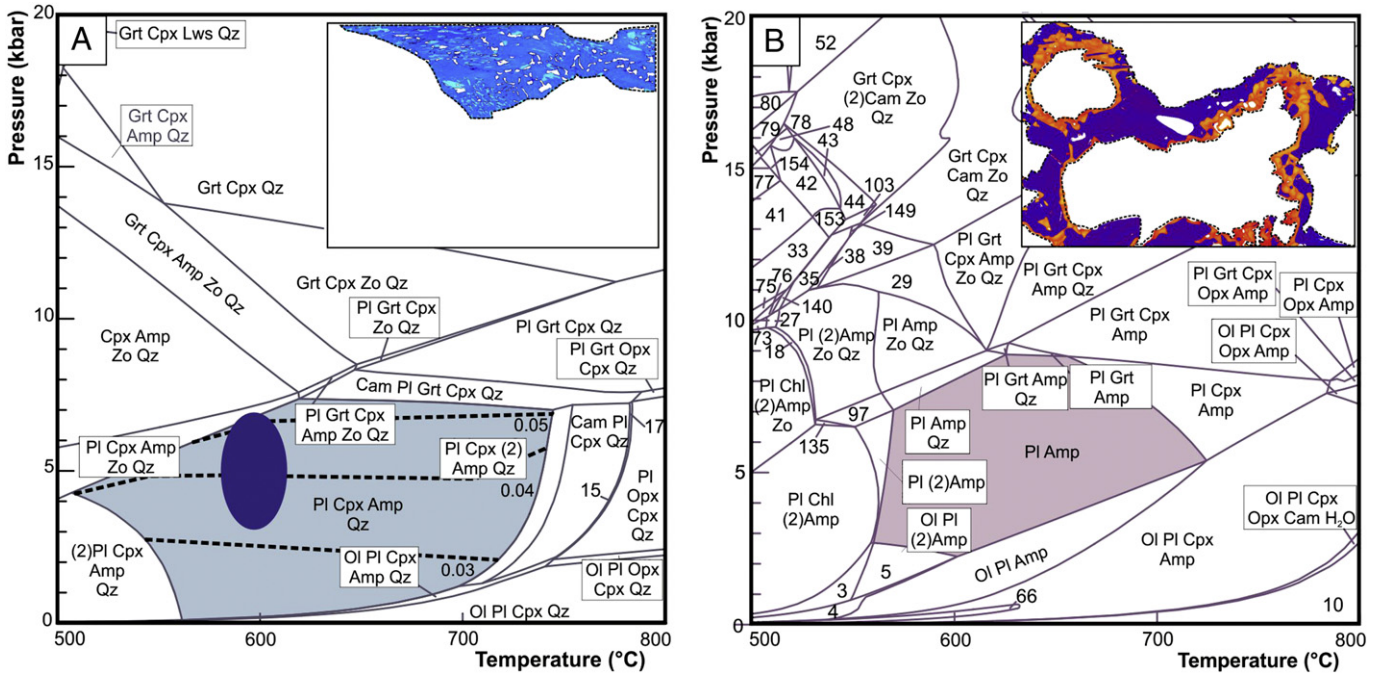

Fig. 6. Pressure-temperature (P-T) diagram calculated for retrieved local compositions from the domains (A) symplectite and (B) for the amphibole + plagioclase corona. Dashed lines in (A) indicate Jd fraction and the blue ellipse represents the P-T conditions obtained from the semi-empirical thermobarometry applying the calibration of Holland and Blundy (1994). Numbered reactions are available on Supplementary Data 7. (For interpretation of the references to colour in this figure legend, the reader is referred to the web version of this article.)

690 ± 35 °C and 13.4 ± 2.8 kbar (Alm_{56} Prp_{18} Grs_{26}) for the average garnet core composition were modelled using the program GrtMod. The mineral assemblage predicted to be stable at these conditions is garnet (34 vol%), clinopyroxene (39%), amphibole (16%), quartz (10%) and rutile (1%). The modelled clinopyroxene composition at 690 °C and 14 kbar has a relatively high Na-content (Jd_{20}).

The bulk rock composition cannot be used to model the reactions that lead to the formation of the symplectite and corona because the evolution of these domains involved local equilibria (Brouwer and Engi, 2005). One way to address this problem is to restrict the analysis to local domains, i.e., to use a local bulk composition as an approximation of the reactive bulk composition. The integration of pixel compositions in specific domains (shown in Fig. 6) after a density correction (Lanari and Engi, 2017) was used to approximate local bulk compositions of the symplectite and the corona. An attempt to reconstruct the composition of Cpx1 from the symplectite local bulk composition returned Si(2)Al(0.20)Mg(0.63)Fe(0.26)Ca(0.76)Na(0.08) in apfu calculated on a basis of 6 oxygen (see Section 5.1.1). Since in a simple ternary clinopyroxene model, Al must be equal to Na and therefore to the jadeite content, Al contours were used to constrain pressure conditions around 14 kbar (Fig. 5). The mineral assemblage composed of clinopyroxene, amphibole, plagioclase and quartz, observed in the symplectite, is predicted to be stable between 500 and 730 °C, 1 and 7 kbar in the corresponding P-T isochemical phase diagram calculated from local bulk rock (Fig. 6A). In this stability field, the modelled clinopyroxene shows low Na-contents (Jd_{3-5}). The range of measured jadeite content in clinopyroxene in this sample allows refining the pressure estimate for the symplectite formation to 6 ± 1 kbar. The mineral assemblage observed in the corona is predicted to be stable between 500 and 700 °C, 2 and 7 kbar (Fig. 6B). The modelled plagioclase composition matches the observations.

For the migmatitic amphibole-garnet gneiss (MT-17) Theriak-Domino was used to model the stable mineral assemblage and phases composition at specific P and T conditions. The chemical system applied was Na_2O–K_2O–CaO–FeO–Fe_2O_3–MgO–Al_2O_3–SiO_2–H_2O–TiO_2 simplified because of the low Mn content in garnet, the main Mn-bearing phase. The internally consistent database applied was TC55, together with the following solid solution models: garnet, biotite and liquid (modified after White et al., 2007); amphibole (Diener et al., 2007); plagioclase (Holland and Powell, 2003); and magnetite (White et al., 2002). The results showed conditions of around 14 kbar and 700 °C.

4.3.2. Mineral thermobarometry

The temperature of amphibole crystallization in sample MT-13 was estimated from the distribution of Na and Ca between plagioclase and hornblende using the edenite-tremolite calibration of Holland and Blundy (1994). The Na-rich amphibole inclusions in garnet yield temperature of 620 ± 47 °C (1σ). Amphibole in the symplectite and corona yields temperatures of 595 ± 26 °C and 600 ± 16 °C, respectively. Following the strategy of Lanari et al. (2013), we determined the pressure of clinopyroxene pixels within the symplectite based on the reaction: jadeite + tremolite = albite + edenite (Waters, 2003). Activities of end members were calculated for amphibole and clinopyroxene following the models of Dale et al. (2000) and Holland (1990), respectively. The pressure estimates range between 3 and 7 kbar with an average of 4.8 ± 1.5 kbar (Fig. 6). The average T and P given here are reported together with a standard deviation value (1σ) obtained from the variability of the P and T maps (see Lanari et al., 2014 for a discussion). This number reflects the relative uncertainty in the estimates that is related to the analytical precision of the EPMA measurements (Lanari et al., 2013).

4.3.3. Rutile thermometry and trace element compositions

Temperature of rutile formation can be determined using Zr-in-rutile thermometry (Tomkins et al., 2007; Watson et al., 2006; Zack et al., 2004). Zr concentration in rutile is dependent on both Si and Zr activities so that thermometry can be only applied in the presence of the appropriate buffering assemblage zircon and quartz. Those phases must have coexisted along in equilibrium with the growing rutile. Rutile LA-ICP-MS trace element analyses were performed to estimate the formation temperature of rutile.

In sample MT-13, metamorphic zircon and quartz are observed in the rock and as inclusions in rutile, suggesting that the activities were buffered. Seventeen analyses on different morphologically grains reveal Zr contents in rutile ranging from 440 to 770 ppm. The input pressures were fixed to 5, 10 and 15 kbar. The corresponding Zr-in-rutile temperatures calculated with the calibration of Tomkins et al. (2007) are 675 ± 16 °C, 701 ± 16 °C and 724 ± 17 °C (1σ) (Fig. 5). Using the calibration of Watson et al. (2006) the Zr-in-rutile temperatures range between 675 and 725 ± 30 °C, with an average of 696 ± 16 °C (1σ).

Most of the analyzed trace elements (22 elements) do not show any correlation with the Zr content and consequently with temperature (e.g., Si, Al, Nb, W, U, Pb). The best positive correlation is observed for Hf (14 to 28 ppm), whereas other elements such as Fe (345 to 13,196 ppm) show a more scattered signal. Nb has concentrations between 322 and 701 ppm, and Cr between 461 and 929 ppm; both elements do not show correlations with temperature.

4.4. U-Th-Pb geochronology and trace elements of zircon and monazite

Isotopic, trace element and inclusion compositional data are reported on Supplementary Data 2 for MT-13, Supplementary Data 3 for MT-22A, Supplementary Data 4 for MT-17, Supplementary Data 5 for MT-19 and Supplementary Data 6 for MT-20.

4.4.1. Clinopyroxene-garnet amphibolite MT-13

Zircons are mainly prismatic, between 120 and 200 μm in length, with length:width ratios of 2:1 and 3:1. Cathodoluminescence imaging reveals parallel oscillatory zoning cores that are surrounded by high luminescent rims, which are variable in thickness and shape. A considerably part of the population exhibits crystals with small remnants of irregularly shaped cores and thick rims. The core-rim boundary is commonly embayed (Fig. 7 and Supplementary Fig. S.7).

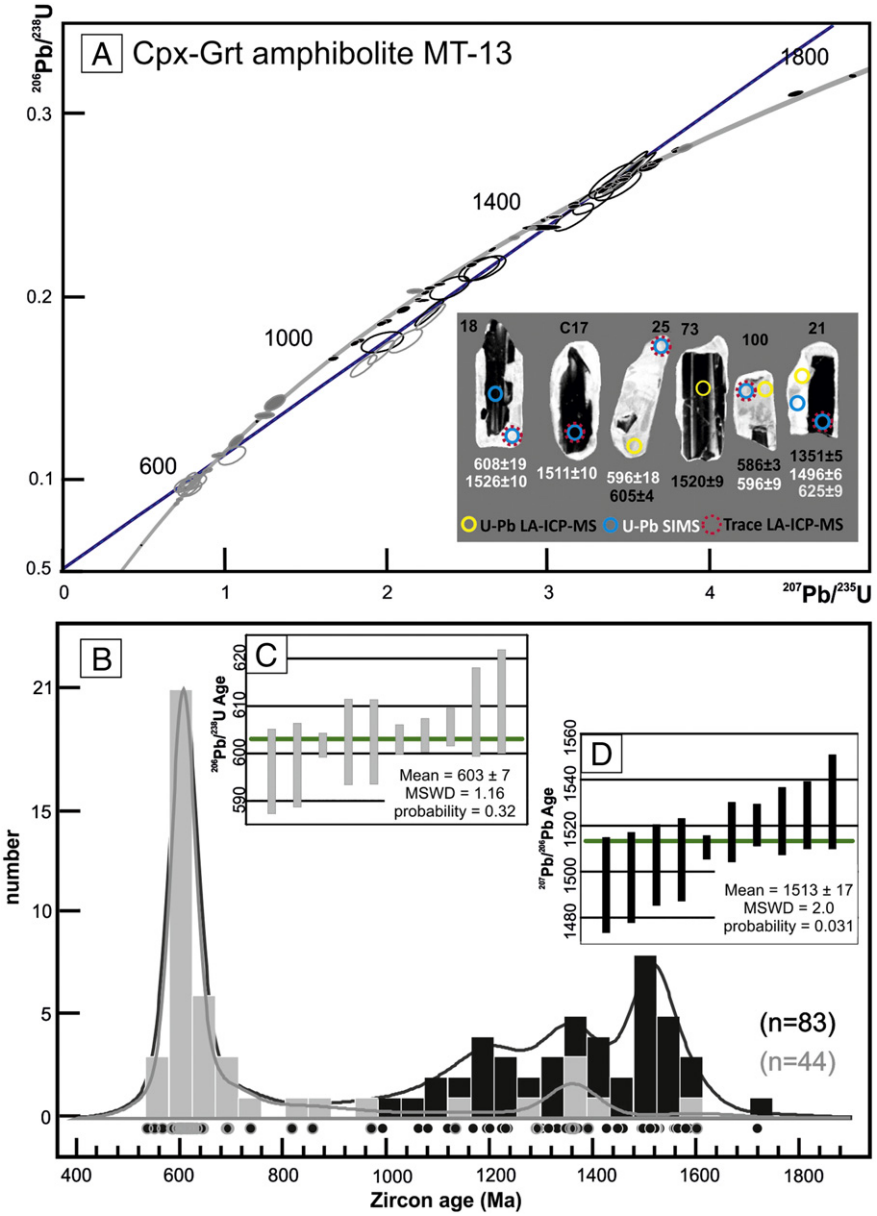

Fig. 7. U-Pb zircon data from clinopyroxene-garnet amphibolite MT-13. (A) Concordia diagram (2σ error ellipses) with CL-images of representative grains analyzed (yellow circle for LA-ICP-MS, blue circles for SIMS analyses and dashed red circles for trace elements, spot size ~25 μm); Filled ellipses for cores analyses LA-ICP-MS (black) and rims (grey) and empty ellipses for SIMS analyses of cores (black) and rims (grey). (B) Kernel density diagram for data considered for age calculation; core data in black and rim data in grey. (C) Data defining the metamorphic age from the weighted average of the rims. (D) Data defining the protolith age. (For interpretation of the references to colour in this figure legend, the reader is referred to the web version of this article.)

Zircon grains were analyzed for U-Th-Pb by SIMS and LA-ICP-MS (141 spots on 87 grains) using the same zircon standard (91,500, reference 1065 Ma, Wiedenbeck et al., 1995). Both methods provided similar results. LA-ICP-MS data were filtered based on common lead content and reproducibility of isotopic ratios within analysis. Th/U ranges from 0.01–1.4 in cores, and 0.01–0.05 in rims and single phase grains (entire crystals which show the same CL-bright response as rims). The data spread along Concordia between a maximal core $^{207}Pb/^{206}Pb$ age of c. 1590 Ma and an age of c. 550 Ma defined by rim analyses (Fig. 7A). The data scatter for both core and rim dates require caution in the interpretation of ages, which are obtained only for the main cluster of dates corresponding to each domain (Fig. 7B). The oldest concordant group of core dates yield an average age of 1513.3 ± 17.1 (MSWD = 2, N = 10; Fig. 10D). Nonetheless, there are cores dates that spread between this age and c. 1600 Ma, with similar CL-responses to the older cores.

Chondrite-normalized (McDonough and Sun, 1995) pattern of core domains (N = 11) have a steep HREE pattern (Fig. 8A), with Lu_N/Gd_N mainly between 16 and 34 and slight to moderate negative Eu anomaly (Eu/Eu* 0.45–0.91). This signature is compatible with a mafic protolith containing little plagioclase. Both cores and rims show a disperse results

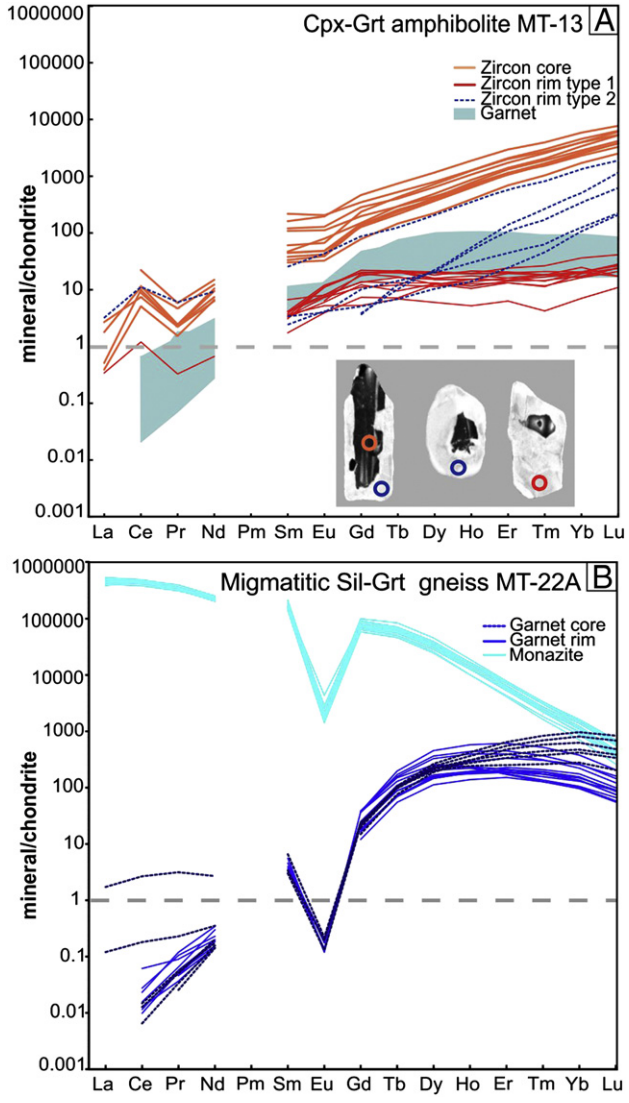

Fig. 8. Chondrite normalized diagrams of the REE composition of: (A) Different dated domains in zircon and garnet from the clinopyroxene-garnet amphibolite MT-13 with location of the analyzed spots in representative grains (spot size ~25 μm); (B) Dated monazite and garnet from the migmatitic sillimanite-garnet gneiss MT-22A. Chondrite normalizing values from McDonough and Sun (1995).

for LREE, especially for La, Ce and Pr, that may indicate the presence of micro-inclusions. Ti was analyzed in the different CL-domains and temperatures were calculated using the Watson et al. (2006) calibration. The eleven cores, with Ti contents between 1.6 and 41.7 ppm, provided temperatures in between ca. 600 and 890 °C. The age of the oldest cluster of core analyses is thus interpreted to date the protolith based on oscillatory zoning, relatively high Th/U, Ti-in-zircon temperatures and high REE content.

The vast majority (c. 80% of a total 46 grains) of zircon rims yield dates between 550 Ma and 700 Ma. The youngest cluster of concordant analyses yield an average age of 603.1 ± 6.8 Ma (MSWD = 1.16, N = 10; Fig. 7B). The intermediate dates that scatter between protolith age and the youngest cluster either describe a Discordia with lower intercept at c. 670 Ma (mainly SIMS analyses), or scatter along Concordia. These intermediate dates are possibly due to partial Pb loss in the cores, incomplete resetting of the U-Pb system in the rims, or physical mixing of core and rim domains during analysis and no geological meaning is attributed to them.

Trace element compositions of zircon rims indicate two patterns for domains that are similar in CL zoning: a) the majority of analyses (N = 13) show a flat HREE pattern, with Lu_N/Gd_N of 0.86–3.75 and moderate negative to slightly positive Eu anomaly (Eu/Eu* 0.65–1.17), b) a few zircon rims (N = 6) have higher Lu_N/Gd_N (20 to 300) and moderate Eu anomaly (Eu/Eu* 0.58–0.75) or low MREE content below the limit of detection (Fig. 8A). For the nineteen zircon rims, the Ti content is in between 1.5 and 21 ppm, with some values under the limit of detection. The resulting Ti-in-zircon temperatures ranges from 590 to 810 °C for rim type 2 (steep HREE), and from 610 to 790 °C for rim type 1 (flat HREE).

Inclusions in zircon have showed to be a valuable tool in connecting P-T conditions to age information (Gilotti, 2013; Hermann et al., 2001; Katayama and Maruyama, 2009), especially in (U)HP rocks in which prograde to peak assemblages are easily replaced during decompression. Oscillatory cores contain numerous sub-μm inclusions of amphibole, clinopyroxene and quartz. Clinopyroxene and amphibole found in the core have high Al_2O_3 and Na_2O, comparable to the values for the reconstructed symplectite composition (see Section 5.1.1) and inclusions in rutile, respectively (Fig. 4). The data from amphibole inclusions in an oscillatory core show a composition of edenitic hornblende (Tindle and Webb, 1994 and references therein). Given the altered nature of the cores (disturbed CL zoning, fractures and disturbed U-Pb ages) the mineral inclusions are interpreted as secondary: they are suspected to have formed in the zircon cores along fractures and zoned of alteration due to fluid infiltration during metamorphism (grains #24 and #47 in Supplementary Fig. S.1).

The zircon rims contain a few 1 and 10 μm sized inclusions of clinopyroxene, amphibole, quartz, garnet and biotite (Supplementary Fig. S.1). Clinopyroxene inclusions in zircon rims show the lowest values of Al_2O_3 and Na_2O among Cpx analyses (including matrix, symplectite, inclusions in rutile and garnet; Fig. 4). Hornblende inclusions have a similar composition to the amphiboles in corona, inclusions in garnet and some of the matrix crystals (Fig. 4). One garnet inclusion has the composition $Alm_{54}Grs_{25}Prp_{18}$ (considering MnO = 1%), the same found for crystals in the matrix.

4.4.2. Gneisses

The migmatitic sillimanite-garnet gneiss MT-22A has zircon grains that are prismatic and elongated (50 to 300 μm). Around 80% of the grains have a CL-dark response, with some oscillatory zoning preserved mainly in the cores (Fig. 9). Similar, mottled, CL-dark zoning has been attributed to metamictization and/or alteration (Corfu et al., 2003; Nasdala et al., 2003). Concordant zircon dates spread between c. 1470–620 Ma with two main clusters at around 670 Ma and 800 Ma. Because of the poor CL zoning, Th/U ratio was the main criteria to distinguish between domains. The eleven younger analyses with Th/U ratios higher than 0.1, and with recognizable oscillatory zoning

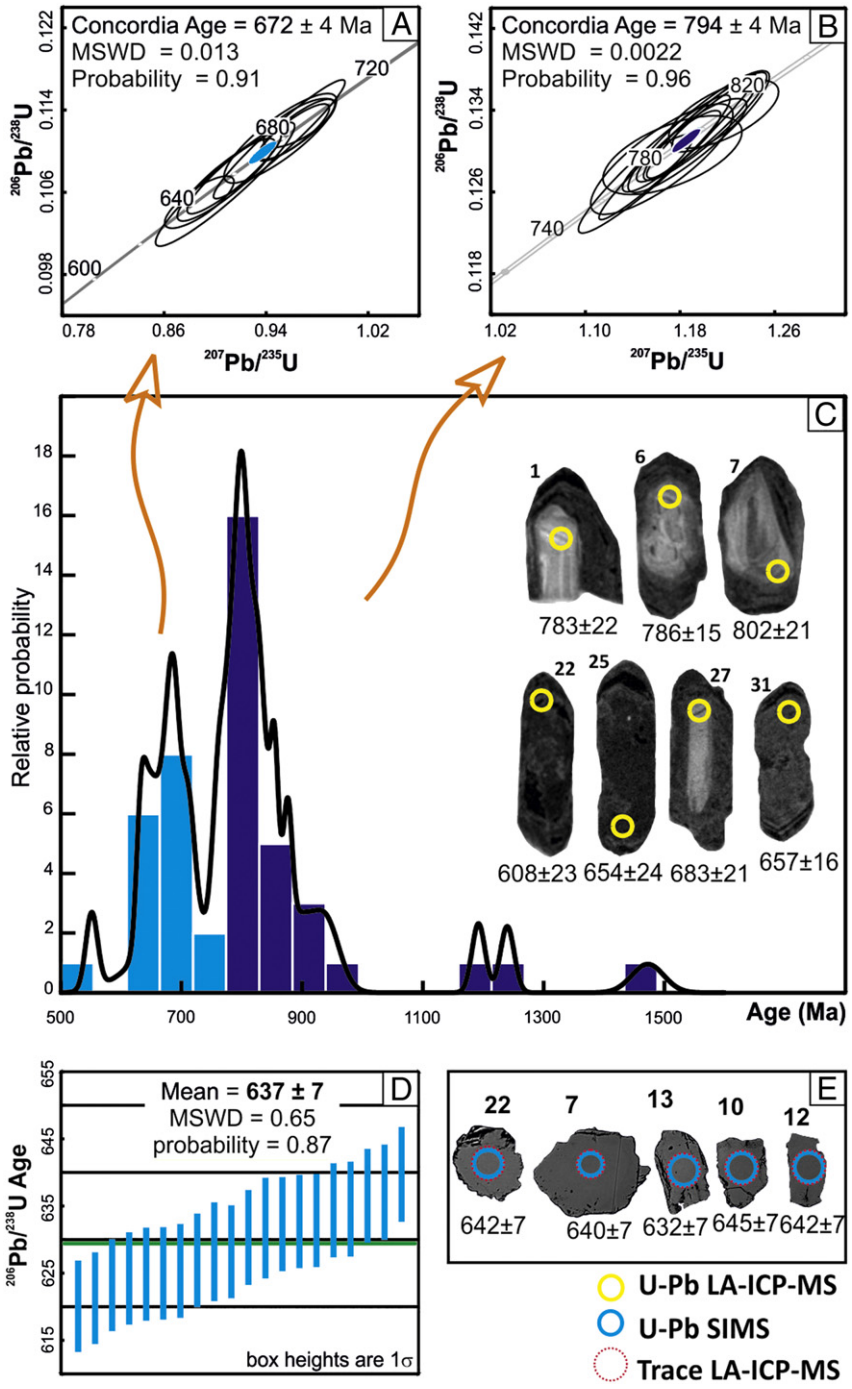

Fig. 9. Geochronological results for migmatitic sillimanite-garnet gneiss MT-22A. (C) Probability density diagrams showing the distribution of the zircon data of the migmatitic sillimanite-garnet gneiss MT-22A and CL-images of representative grains analyzed (spot size ~25 μm). The light blue bars indicate the data with low Th/U ratios, used for calculating the metamorphic age from the Concordia diagram in A. (B) The Concordia diagram for the grains with Th/U ratios higher than 0.1, from which the main data peak defines the maximal depositional age. (D) Weighted average $^{206}Pb/^{238}U$ ages diagram for monazite, and (E) backscattered electron images of representative grains analyzed on the Concordia diagrams (ellipses are 1σ error). (For interpretation of the references to colour in this figure legend, the reader is referred to the web version of this article.)

are interpreted as magmatic and provide a concordia age of 793.8 ± 3.9 Ma (Fig. 9). Zircon euhedral morphology and the cluster of ages for preserved magmatic zircons suggest that this rock had mainly one zircon source. Zircon domains with low Th/U ratios yield dates ranging mainly from 940 to 550 Ma with a major cluster of nine analyses constraining a concordia age of 671.8 ± 3.8 Ma. Such analyses were mostly located in the external portion of the crystal.

Monazite grains in the gneiss are clear, light yellow, anhedral and smaller than 150 μm (Fig. 9). The crystals do not display any internal structure in BSE imaging. Twenty grains analyzed by SIMS have an average $^{206}Pb/^{238}U$, age of 636.5 ± 7.2 Ma (MSWD = 0.65; 95% c.l.; Fig. 9). Chondrite-normalized REE patterns on sixteen monazite grains show homogeneous compositions. Crystals have the expected signature for monazite with strong enrichment in LREE (La ~500,000), a progressive depletion in HREE (Gd/Lu 111–245) and strong negative Eu anomaly (Eu/Eu* 0.01–0.04), as described in previous works (Hermann and Rubatto, 2003; Rubatto et al., 2006) (Fig. 8B).

In the migmatitic amphibolite-garnet gneiss MT-17 zircon grains range in size from 100 μm to 400 μm. Most grains show oscillatory zoning with CL-medium-bright responses. Irregularly shaped CL-dark

cores, as well as discrete few μm thick CL-dark rims, are found in some of the grains (Fig. 10A). Forty-seven LA-ICP-MS analyses on oscillatory domains yield Th/U ratios between 0.31 and 0.74. Most analyses (87%) define a concordia age of 2065.6 ± 2.3 Ma (Fig. 10A), interpreted as the crystallization age of the photolith.

In the allanite-bearing biotite granite MT-19 zircon grains are elongated prismatic, up to 400 μm in length with oscillatory zoning in the majority of the grains. A subset of grains has CL-dark domains combined with poorly zoned rims brighter in CL images (Fig. 10C). Seventy-two analyses were obtained by LA-ICP-MS. Oscillatory cores have Th/U mostly in the range 0.10–0.35 and 0.01–0.18 for the rims. On a Concordia diagram the data separate in two well-defined groups, with 90% of the data around 2 Ga. We adopt the approach used by Whitehouse and Kemp (2010), and consider the largest group of older dates to be significant. In this group, the oscillatory domains provide a concordia age of 2076.1 ± 3.2 Ma (Fig. 10C) with some scattering data down to c. 2.0 Ga. Based on the zoning of the crystals, this age is interpreted as dating the crystallization of the protolith. A discrete group of analyses on rims with low Th/U

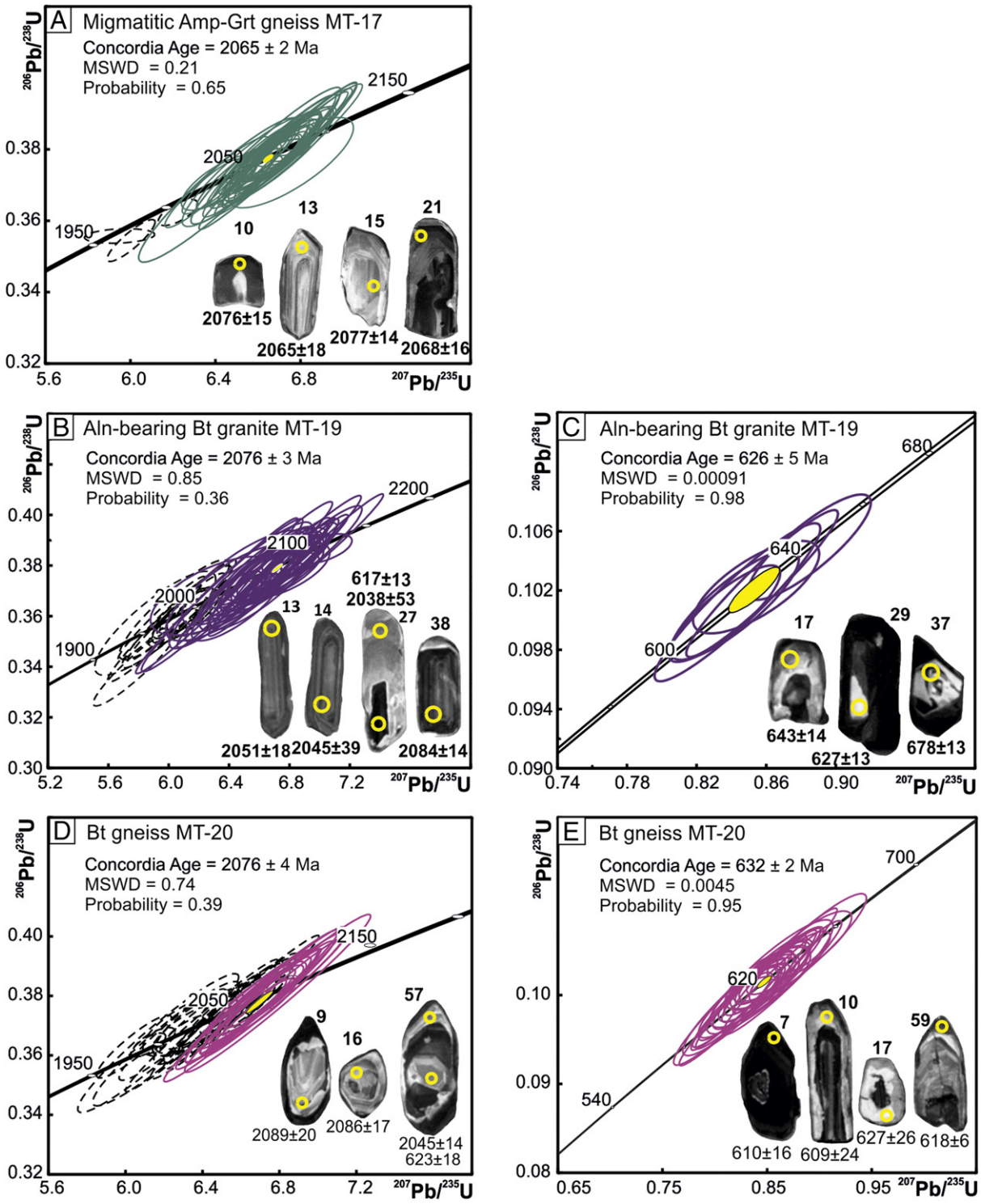

Fig. 10. Geochronological results (LA-ICP-MS analyses, 1σ error ellipses) for migmatitic amphibole-garnet augen gneiss MT-17, allanite-bearing biotite granite MT-19 and biotite gneiss MT-20 with CL-images of representative analyzed grains. In the Concordia diagrams younger analyses discarded are represented by dashed lines (see text for explanation).

yield a concordia age of 626 ± 5 Ma that is interpreted to be related to a metamorphic event (Fig. 10D).

Biotite gneiss MT-20 has a heterogeneous zircon population, with most grains showing multiple domains in CL. Generally, complex cores have various CL zoning that in most crystals is truncated by rims with weak or no regular zoning and variable CL-emission (Fig. 10E). Seventy-three analyses in fifty-six grains were carried out with LA-ICP-MS. Th/U ratios range mainly between 0.15 and 0.84 for the cores, and <0.01 for the rims. Similarly to MT-19, the analyses define two major clusters in the Concordia diagram, but with a most representative cluster for younger ages (c. 600 Ma). With a similar approach as described for MT-19, the fifteen older analyses corresponding to zircon cores define a concordia age of 2076.2 ± 4.4 Ma (Fig. 10E). A coherent group of twenty-eight overgrowths with Th/U < 0.1 yielded a concordia age of 632.2 ± 2.4 Ma (Fig. 10F). Ages are interpreted, based on internal zoning and Th/U composition, to constrain the Paleoproterozoic age of the protolith and a Neoproterozoic metamorphism.

4.5. Garnet trace element composition

4.5.1. Clinopyroxene-garnet amphibolite MT-13

Corroborating the major element compositional maps, eighteen trace elements spot analyses reveal a homogeneous composition for garnet crystals. Chondrite-normalized (McDonough and Sun, 1995) garnet patterns show LREE depletion ($La–Sm_N$ 0.01–0.53; Some La, Ce and Pr concentrations are under detection limit), slight to moderate negative Eu anomaly (Eu/Eu* 0.54–0.84) and relative flat HREE enrichment (Lu/Gd_N 0.73–2.34; Fig. 8A).

4.5.2. Migmatitic sillimanite-garnet gneiss MT-22A

Twenty garnet analyses (Fig. 8B) reveal a significant variation between core and rim. The cores are enriched in heavier elements (e.g., Ho, Er, Tm, Yb and Lu; Lu/Gd_N 1.43–37.07), while the rims display a convex shape with depletion in these elements (Lu/Gd_N 2.66–14.53). The analyses show a discrete spread in LREE (Ce 0.006–0.18) and a marked negative Eu anomaly (Eu/Eu* 0.005–0.015, only 30% of Eu analyses are above detection limit). LREE depletion below chondrite values, strong negative Eu anomaly and relative HREE enrichment are typical for high-grade metamorphic garnet from granulites or migmatites (Hermann and Rubatto, 2003; Kelly and Harley, 2005; Rubatto et al., 2006).

5. Discussion

5.1. Petrochronological evolution of clinopyroxene-garnet amphibolite MT-13

5.1.1. Pressure peak conditions

Garnet thermobarometry indicates growth conditions of 690 ± 35 °C and 13.4 ± 2.8 kbar for the average garnet core composition. The absence of strong major element compositional zoning in garnet might be interpreted as a direct consequence of intragranular diffusion that enhanced re-equilibration of the small crystals in equilibrium with the omphacitic matrix near the peak conditions. Theoretical models show that the time required to produce unzoned crystals of 2–3 mm size is in the order of 10–50 Ma (Caddick et al., 2010) for metamorphic temperatures around 690 °C. Age dating results (see below) suggest that this sample might have experienced more than 20 Ma at conditions hotter than 600 °C (Coelho et al., 2017; and results from this study). In this case any prograde growth zoning would be significantly affected by diffusion and the final garnet composition may eventually reflect (partial) equilibrium conditions at HT conditions. Alternatively, the garnet completely recrystallized at peak metamorphic conditions, also equilibrating any zoning in trace elements. At these conditions, the metamorphic assemblage predicted to be stable in a rock of this composition consists of garnet, clinopyroxene, amphibole, rutile and quartz. This HP assemblage has been strongly retrogressed into symplectite and coronas and the comparison between modelled and measured clinopyroxene composition shows that the former omphacite (Cpx1) was completely re-equilibrated after the HP stage (Fig. 4). Comparing the integrated composition of Cpx1 from the symplectite domain using the average composition determined from the compositional maps (see Section 4.3.1) returned Si(2)Al(0.20)Mg(0.63)Fe(0.26)Ca(0.76)Na(0.08) in apfu and, the composition of Cpx1 predicted by the model at 690 °C and 13.4 kbar is Si(2)Al(0.19)Mg(0.59)Fe(0.22)Ca(0.81)Na(0.19). The two compositions are fairly similar with the exception of Na that appears to be significantly lower in the symplectite. In a simple ternary clinopyroxene model, Al must be equal to Na and therefore to the jadeite content. As (1-Ca) ≈ Al in the symplectite composition, we can assume that the symplectite formed from a HP omphacite with a $Jd_{20–21}$ composition. In this scenario, Na was lost during the symplectite formation, whereas Si, Al, Fe and Mg were kept unchanged.

A Zr-in-rutile temperature of 701 ± 16 °C (1σ) was determined at a pressure of 10 kbar using the calibration of Tomkins et al. (2007). The temperature range is in agreement with the conditions derived for the garnet core. The homogeneous distribution of Zr in rutile suggests that rutile grew in a narrow range of temperature. The P-T diagram indicated that rutile occurs above 9 kbar. The inclusions in rutile, such as amphibole, plagioclase, titanite and clinopyroxene ($Jd_{9–4}$), suggest a lower pressure around 5–9 kbar (Fig. 5). Amphibole and clinopyroxene inclusions in rutile have a different composition compared to the grains preserved in the mineral matrix. Clinopyroxene shows higher XMg (~0.76) and amphibole higher Na_2O and Al_2O_3 contents (Fig. 4), reflecting a different coexisting metamorphic assemblage. Based on these observations, rutile is interpreted to have grown during burial from 9 to 14 kbar at 675–720 °C. The presence of rutile inclusions in garnet supports the scenario of growth before or together with garnet.

Apart from rutile, garnet is the only remnant of the higher-pressure stage in this rock and therefore the maximal estimate of 13.4 ± 2.8 kbar is based on garnet thermobarometry. Omphacite (Cpx1) is no longer preserved, but reconstruction from the composition of the symplectite shows that Jd_{20} omphacite may have coexisted with this garnet at similar pressure conditions. If the sample would have reached higher pressure, this could have been recorded by inclusions trapped in the accessory minerals. Inclusions in rutile indicate a lower grade metamorphic assemblage (prograde) as for zircon (retrograde). We conclude that there is no evidence that the mafic rock MT-13 reached pressures higher than 14 kbar. Therefore, this sample is better classified as a high-pressure (HP) amphibolite, instead of "retro-eclogite".

5.1.2. Formation of symplectite and corona and implications for element mobility

The HP assemblage of garnet, omphacite, amphibole and quartz was partially transformed into two retrogression products: symplectite and corona. The symplectite consists of clinopyroxene, amphibole and plagioclase, and has formed through the destabilization of a former omphacite (Cpx1), following the reaction:

$$\text{R1: Cpx1} + H_2O = \text{Cpx2} + \text{Amp2} + \text{Pl} \pm \text{Qz} + Na_2O \quad (1)$$

Similar reactions have been observed in retrogressed mafic eclogites (Lanari et al., 2013; Waters, 2003). The corona is made of plagioclase and amphibole and has formed through the reaction:

$$\text{R2: Grt} \pm \text{Amp1} \pm \text{Cpx1} \pm H_2O = \text{Amp2} + \text{Pl} \quad (2)$$

with unconstrained proportions of amphibole (Amp1) and clinopyroxene (Cpx1). A significant fraction of garnet may have been dissolved during the formation of the corona.

The P-T conditions of formation of these two domains have been estimated by using local bulk compositions to approximate their reactive bulk compositions (Lanari and Engi, 2017). This strategy relies on the

assumption of thermodynamic equilibrium, whereas the investigated domains preserve strong evidence of frozen-in chemical potential gradients. Nevertheless, the equilibrium models predict modal abundances and mineral compositions that are in line with the observation such as the average compositions of mineral phases determined in each domain. Any spatial organization or compositional zoning caused by chemical potential gradients within a single domain cannot be modelled by this technique and, therefore, requires the use of μ-μ diagrams (White et al., 2008). However, the alternative strategy described in this study does not require any kinetic assumption such as immobile Al_2O_3, providing an estimate of the average physical and chemical conditions in each domain.

Amphibole thermometry and clinopyroxene barometry have been applied to the minerals located in the symplectite and corona. This inverse method can be used to obtain P-T conditions from retrogressed domains (Lanari et al., 2013; Loury et al., 2016; Waters, 2003). The symplectite formed at 595 ± 26 °C and 4.8 ± 1.5 kbar, in good agreement with the results of the forward equilibrium models (Fig. 6A). A temperature of 600 ± 16 °C has been estimated for the corona. No pressure data could be obtained because of the absence of clinopyroxene. At this temperature, the pressure is fixed by the geometry of the stability field of plagioclase + amphibole at 5 ± 2.5 kbar (Fig. 6B). Symplectite and corona have thus formed at similar P and T conditions along the retrogression. Titanite corona around rutile, and locally ilmenite, suggests a similar path in the P-T diagram (Fig. 5).

It is interesting to evaluate the possible element exchanges occurring between the two domains – symplectite and corona – during retrogression. This can be analyzed in Al_2O_3 against Na_2O binary diagrams that consider bulk rock, symplectite, corona and mineral compositions for the peak and retrograde stages (Fig. 11). The bulk rock composition correctly lies between composition of the modelled peak minerals (Fig. 11A), and in between that of retrograde garnet, symplectite and corona (Fig. 11B). Reaction R1 is well constrained as the composition of Cpx1 can be derived from the model at 690 °C and 13.4 kbar (Section 5.1.1). From Fig. 11B, it can be deduced that about ~2 wt% of Na_2O is released from the reaction R1: Cpx1 → symplectite. The reaction R2 is more difficult to constrain because it is not possible to evaluate the bulk composition of the reactants. However, the texture suggests that the corona formed from garnet and amphibole1 (±Cpx 1), marked by the mixing line shown in Fig. 11B (dashed grey line). For a reacting volume made of amphibole (80 wt%) and garnet (20 wt%), the formation of the corona requires a gain of ~2 wt% of Na_2O at a fixed value of Al_2O_3. Then, the reaction R2 can be refined as:

$$R2: Grt \pm Amp1 \pm Na_2O = Amp2 + Pl \quad (3)$$

This mass balance model shows that the two reactions were coupled. The excess of Na released from the symplectite reaction corresponding to 2.1 g of Na_2O per 100 g of the parent omphacite (assuming no volume change) is required to drive reaction R2 and develop the corona. These reactions do not require any mobility of Al, and presumably other immobile elements, such as trace elements, between the two reacting domains. The likely immobility of trace elements at this stage has implications for zircon-garnet trace element correlation (see below).

5.1.3. Age constraints and link to P-T conditions

The age of zircon rims in mafic sample MT13 is determined from the youngest cluster of concordant analyses at 603 ± 7 Ma. It is important to link this age to a metamorphic stage.

The CL-bright zircon rims with low Th/U show trace elements patterns that are either flat (type 1) or enriched in HREE (type 2, Fig. 8A). The depletion of HREE and the absence of negative Eu anomaly are commonly attributed to presence of garnet and absence of plagioclase in the coexisting assemblage (Ganade de Araujo et al., 2014; Rubatto, 2002). The absence of Eu anomaly in the zircon rims can be explained by a bulk rock composition effect, as no Eu anomaly is observed in zircon cores (Rubatto, 2017), which presumably grew in a gabbroic protolith in the presence of plagioclase. Therefore, the absence of Eu anomaly in this case is not indicative of zircon growth under plagioclase free, eclogite facies conditions.

Zircon depletion or enrichment in HREE is linked to garnet stability, as garnet is a major carrier of HREE. In this rock sample, however, where chemical equilibrium was essentially localized (see above formation of symplectite and corona) trace element equilibrium between phases in different domains cannot be expected. Garnet textures indicate that garnet has been resorbed during the formation of the corona. Only the zircon growing in a corona would thus incorporate the HREE from garnet. Zircon type 2 has a HREE enriched pattern and possibly formed within a corona while garnet was being dissolved. Retrograde titanite is a potential repository for LREE and MREE and might contribute to the steep pattern of zircon-rim type 2. Type 1 zircon has a flat HREE pattern and could thus have formed before garnet resorption, or in a different domain where garnet was not resorbed, i.e., in the symplectite domain. Zircon rim type 1 and type 2 were never observed in the same grains, and can be related to two different populations. The possibility that type 2 zircon represents mixing analyses between 1.5 Ga core and type 1 rim is excluded by the fact that type 2 analyses do not show older, thus mixed ages. Similar conclusions can been drawn from the dataset of Coelho et al. (2017) in which zircon rims show HREE enrichment but never have ages older than 625 Ma. Therefore, we propose that zircon type 1 and 2 grew in different domains with different local

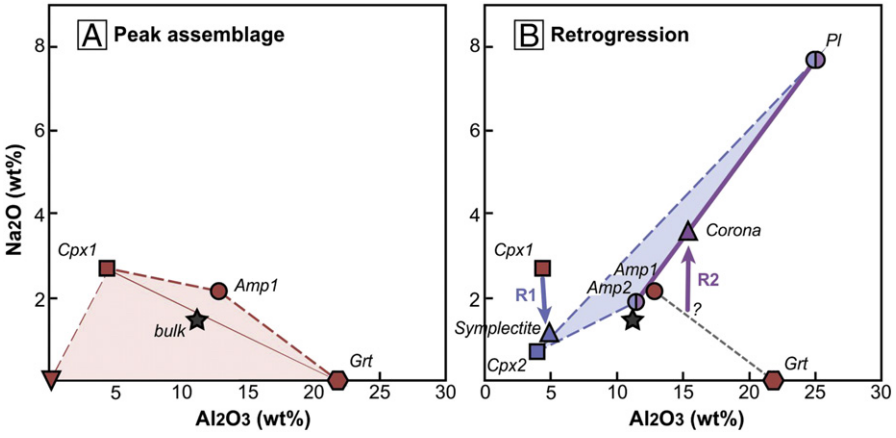

Fig. 11. Al_2O_3 vs Na_2O binary diagram showing the stable phases and their relationship with the bulk-rock (A) at peak conditions and at (B) the retrogression stage. The diagrams show the possible element exchanges occurring between the symplectite and corona domains during retrogression. See text for details.

bulk compositions, most likely during retrogression and the formation of symplectite and corona.

This interpretation is also supported by the analyses of inclusions in zircon rims. Clinopyroxene and amphibole inclusions in zircon show similar compositions to that of minerals in the symplectite and corona (Fig. 4). A single inclusion of omphacite in zircon core shows similar Al_2O_3 to the average composition of the reconstructed symplectite (interpreted as Cpx1). As zircon cores show typical magmatic features and have ages around 1.5 Ga, this inclusion is interpreted as a secondary inclusion formed during metamorphism and alteration of zircon cores, as reported in other metamorphic rocks (Rubatto, 2017).

In conclusion, metamorphic zircon formation in the mafic rock occurred from c. 630 to c. 600 Ma and registers the metamorphic evolution from peak to decompression. The age of 603 ± 7 Ma defined by a cluster of rim dates can be linked to the retrogression stage involving symplectite and corona growth. The results of this study are in line with the predictions by the model of Kohn et al. (2015), showing that zircon is likely to grow under retrograde conditions when garnet is dissolved.

5.2. Magmatic and metamorphic history of the Pouso Alegre rock assemblage

The Pouso Alegre rock assemblage is composed of three distinct rock units that were associated during Neoproterozoic tectono-metamorphic events. These units are: 1) the Paleoproterozoic migmatite, orthogneiss and granite of the regional basement (samples MT-17, MT-19 and MT-20); 2) Mesoproterozoic mafic rocks metamorphosed to clinopyroxene-garnet amphibolite (MT-13) that were previously classified as "retro-eclogite" (Fig. 1C and D); and, 3) a Neoproterozoic peraluminous gneiss of uncertain origin (migmatitic sillimanite-garnet gneiss, MT-22A).

5.2.1. Formation and evolution

5.2.1.1. Paleoproterozoic rock assemblage. The migmatitic amphibole-garnet gneiss MT-17, allanite-bearing biotite granite MT-19 and biotite gneiss MT-20 have magmatic zircon or zircon cores dates at 2065 ± 2 Ma, 2076 ± 3 Ma and 2076 ± 4 Ma, respectively (Fig. 12). The three gneisses show similar ages, as well as mineralogical and major element compositions, but distinct trace element signatures for HREE (Supplementary Fig. S.2 and Supplementary Data 1), suggesting that they are members of a Late Rhyacian magmatic suite. The ages of c. 2.07 Ga and field relations suggest that these rocks belong to the Pouso Alegre complex, a basement unit of the reworked margin of the São Francisco craton (Cioffi et al., 2016). The bulk rock chemistry of the migmatitic amphibole-garnet gneiss and biotite gneiss are compatible with the granodioritic and granitic samples described by Cioffi et al. (2016), as showing juvenile Hf and Nd signatures. Trace element signatures from sample MT-17 and MT-20, are in accordance to those from granites and granodiorites of the Pouso Alegre basement, which in turn resemble subduction-related patterns of modern arcs (Cioffi et al., 2016). However, the allanite-bearing biotite granite MT-19 is depleted in HREE, suggesting that it represents a melt from a source that retained significant amount of garnet, possibly a metasedimentary rock (cf. Wilson, 1989).

5.2.1.2. Clinopyroxene-garnet amphibolite MT-13. It forms a steep-dipping concordant body hosted by saprolites from migmatitic-gneissic rocks, most probably correlated with the orthogneisses of the Rhyacian Pouso Alegre complex (see Section 3). The bulk rock chemistry indicates a tholeiitic composition for the protolith, with a signature between N-MORB and *E*-MORB. REE patterns for the magmatic zircon cores (Fig. 8) show a small Eu anomaly, supporting a basaltic liquid composition for the protolith, with minimal plagioclase fractionation. Kaczmarek et al. (2008) reported similar trace element signatures in partly metamorphosed zircon grains from metagabbros. Ti-in-zircon

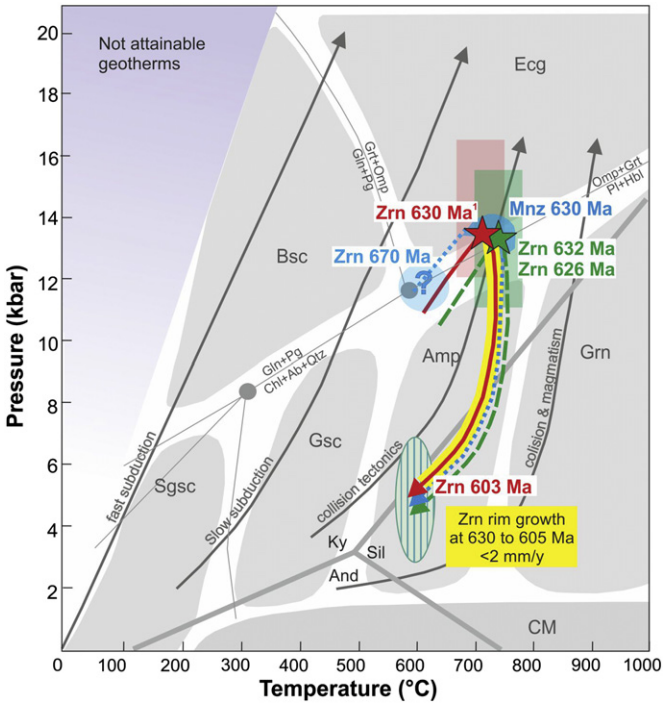

Fig. 12. P-T-t trajectories for the clinopyroxene-garnet amphibolite MT-13 (red), migmatitic amphibole-garnet gneiss MT-17 (green) and migmatitic sillimanite-garnet gneisses MT-22A (blue); stars represent the P-T condition and rectangles their uncertainties. The ellipse filled with stripes represents the symplectite conditions of formation, which are the same as for corona. Zircon age of 630 Ma is from Coelho et al. (2017) which investigated a similar sample. The 670 Ma from zircon grains of the migmatitic sillimanite-garnet gneiss MT-22A cannot be strictly correlated to a P-T condition (thus indicated by "?"). See text for discussion of the ages. Metamorphic facies grid for metabasaltic rocks and geothermal gradients from Bucher and Frey (2002); CM – Contact metamorphism, Grn – Granulite, Amp – Amphibolite, Gsc – Greenschist, Sgsc – Subgreenschist, Bsc - Blueschist. (For interpretation of the references to colour in this figure legend, the reader is referred to the web version of this article.)

temperatures are spread, but show highest values around 900 °C, compatible with crystallization of residual basaltic magmas after crystallization of cumulus phases.

The chemistry, an age that is 900 My older then the collision event, together with its location in a continental section, argue for a continental rift origin rather than a relic oceanic crust. The significant amount of magmatic zircon grains found in this mafic rock, as well as their morphology, suggests that the photolith was a plutonic to subvolcanic rock. Zircon cores constrain a minimum crystallization age at 1513 ± 17 Ma, in line with the 1504 ± 29 Ma age reported by Coelho et al. (2017) for mafic rocks from Pouso Alegre. In conclusion, we suggest that the clinopyroxene-garnet amphibolite represents a tholeiitic magma that intruded the Rhyacian basement during a c. 1.5 Ga extensional episode possibly correlated to Calymmian (1.6–1.4 Ga) rifting events known in the region (e.g., Heilbron et al., 2017).

5.2.1.3. Migmatitic sillimanite-garnet gneiss MT-22A. The presence of garnet and sillimanite indicates an aluminous protolith that could be either sedimentary or granitic. The zircon population is homogeneous, with euhedral elongated crystals and a single age of 794 ± 4 Ma. These features are in line with a magmatic protolith, but could also be compatible with a volcanoclastic sediment. Ages around 800 Ma have been reported as detrital zircon grains from metasedimentary rocks of the Andrelândia nappe system and nearby units (Belém et al., 2011; Trouw, 2008; Westin et al., 2016). However, contrasting to the narrow zircon age distribution shown by the migmatitic sillimanite-garnet gneiss MT-22A, those samples show large age spectra, spreading from the Cambrian to the Paleoproterozoic with relatively few grains around 800 Ma, like the Santo Antônio schist (Belém et al., 2011) and the

Arantina unit (Coelho et al., 2017). Those units have been interpreted as sedimentary deposits related to passive or active margins (e.g., Belém et al., 2011; Coelho et al., 2017). The period of c. 900–700 Ma has been associated with continental rifting to ocean opening events (Heilbron et al., 2017). However, primary magmatic sources for the c. 800 Ma zircons remain unknown in the Southern Brasília orogen. Therefore, a first finding of such a source could be represented by the sillimanite-garnet migmatitic gneiss MT-22A dated at 794 ± 4 Ma.

5.3. P-T-t record of a common metamorphic history

Zircon rims interpreted as metamorphic (based on both texture and Th/U composition) yield identical ages for the allanite-bearing biotite granite MT-19 (626 ± 5 Ma) and the biotite gneiss MT-20 (632 ± 2 Ma; Fig. 10). No appreciable metamorphic zircon was found in the migmatitic amphibole-garnet gneiss MT-17. The similar protolith age for the three samples suggests that they constituted a unique basement and thus also the migmatitic amphibole-garnet gneiss underwent metamorphism around c. 630 Ma. P-T estimates for migmatitic amphibole-garnet gneiss MT-17 are 13.5 kbar and 700 °C, in line with the conditions of the clinopyroxene-garnet amphibolite MT-13.

In the migmatitic sillimanite-garnet gneiss MT-22A, zircon rim domains with low Th/U are dated at 672 ± 4 Ma, whereas monazite is 637 ± 7 Ma. Monazite has a trace element composition that is relatively poor in HREE and thus is consistent with growth in an assemblage containing garnet (Rubatto et al., 2006). Monazite/garnet distribution coefficients for trace elements have been calculated using the average composition of the monazite (limited compositional variation), and garnet core (Yb $D_{Mnz/Grt} = 2.8$) and rim (Yb $D_{Mnz/Grt} = 7.3$) compositions. Monazite-garnet partitioning for HREE is generally reported as in favour of monazite, with monazite/garnet Yb between 3.8 and 5.3 (Hermann and Rubatto, 2003; Rubatto et al., 2006). The REE zoning in garnet shows depletion from core to rim, with only the garnet rim containing less HREE, specifically Lu, than the monazite. Therefore, the growth of monazite in this sample is correlated to the garnet rim. No P-T conditions can be constrained for this sample. However, its spatial location, as well as the same metamorphic age, point to an evolution together with the other studied rocks. The peak pressure conditions for this rock would thus be in the kyanite stability field, and sillimanite would form during decompression, as described in the literature for rocks of similar composition, the high pressure granulites from the Andrelândia nappe system (Cioffi et al., 2012).

The age of the low Th/U zircon domains is not straightforward to interpret because of the quality of the material analyzed and the difference with the monazite age. This age is defined by a number of analyses on zircons that have dark and mottled CL zoning, which is commonly attributed to alteration (Corfu et al., 2003). If these zircon domains result from partial alteration of the magmatic cores, then the constrained age is a maximal age for the alteration event. Thus, this age constrain is tentatively attributed to an earlier stage of metamorphism around 672 ± 4 Ma or older, maybe related to the garnet core formation.

Similar prolonged metamorphic event, between c. 630 Ma and 600 Ma, has been identified in the Socorro-Guaxupé nappe, however for distinct P-T conditions of c. 1000 °C and 12 kbar (Rocha et al., 2016). Moreover, similar P-T path, with peak conditions around 14 kbar and 700 °C followed by nearly isothermal decompression are recorded by rocks from the Andrelândia nappe system (Coelho et al., 2017; Motta and Moraes, 2017) with metamorphic ages within the 630–600 Ma interval.

5.4. Collision versus subduction setting

The reconstructed P-T-time path for the Pouso Alegre mafic rock and country gneisses (Fig. 12) indicate maximal pressure and temperature conditions at the amphibolite-eclogite boundary followed by near-isothermal decompression. This cooling/exhumation path provides important constraints on geothermal gradients, and metamorphic rates for the Southern Brasília orogen.

The maximal P-T correspond to a geothermal gradient of ~50 °C/kbar and a crustal thickness of ~40 km, using an average crustal density of 2700 kg m^3. While this is a relatively low geotherm compared to stable cratons, this geotherm is comparable to what is observed in collisional belts (Brown, 2007; Sizova et al., 2014). HP and UHP rocks related to subduction evolve along cooler geotherms of <35 °C/kbar (Brown, 2007, 2009; Weller and St-Onge, 2017).

Decompression from ~14 to 5 kbar over c. 30 My results in an average exhumation rate of 1 mm y^{-1}. Such rates would be compatible with erosion-driven exhumation (Burbank, 2002; Schlunegger and Willett, 1999). However, the limited cooling during exhumation suggests a tectonic process, whereby rock units move upwards crossing different geothermal gradients. This is commonly observed in the dynamic exhumation of collisional belts, e.g., in the Himalaya (Chakraborty et al., 2017; McClelland and Lapen, 2013). The second stage (~600 °C and 4.5 ± 1.5 kbar) is close to a typical post-collisional geotherm of ~90–130 °C/kbar (or ~25–35 °C/km; Schlunegger and Willett, 1999) and may represent the onset of a post-orogenic stabilization.

Based on these results, we conclude that the Pouso Alegre HP mafic rocks, previously called "retro-eclogites" cannot be considered as evidence for the southern extension of the West Gondwana UHP belt proposed by Ganade de Araujo et al. (2014). However, those rocks can represent relatively HP metamorphic products from mafic intrusions in a continental setting, metamorphosed in the deep root of the Ediacaran continent-continent collisional zone.

6. Conclusions

The Pouso Alegre rock assemblage is composed of intermediate to felsic rocks that formed at c. 2.07 Ga and were intruded by gabbros at c 1.5 Ga. This igneous complex was overlain by an aluminous volcanoclastic or igneous body at around 800 Ma. Together, those rocks experimented a roughly synchronous metamorphic event in the Brasiliano orogeny, attaining a collisional metamorphic peak around 630 Ma and retrogression conditions around 600 Ma.

The metamorphic evolution of the clinopyroxene-garnet amphibolite was reconstructed using an approach that combines compositional mapping and thermobarometry of targeted textural domains. The methodology employed for the clinopyroxene-garnet amphibolite, which displays typical textures found in decompressed eclogite, allowed reconstructing peak metamorphic conditions, of 13.5 ± 3.0 kbar and 700 °C. The surrounding migmatitic garnet-amphibole gneiss record similar P-T conditions. This metamorphic stage was dated at c. 630 Ma by zircon rims in the country rock gneisses MT-19 and MT-20, monazite from the aluminous gneiss MT-22A, and some zircon rims in the clinopyroxene-garnet amphibolite MT-13. Reconstructions of local domain compositions were used to determine P-T conditions of formation of late stage symplectite and corona at 4.8 ± 1.5 kbar and temperatures between 595 and 600 ± 26 °C. The symplectite of Cpx2 + Amp2 + Pl ± Qz and coronas of plagioclase and amphibole around garnet formed in coupled reactions involving Na exchange. Metamorphic zircon rims from the clinopyroxene-garnet amphibolite constrain decompression at these conditions around 603 ± 7 Ma.

The high geothermal gradient from the clinopyroxene-garnet amphibolite is not compatible with a subduction gradient, but rather indicates metamorphism related to continent-continent collision tectonics. Hence, the Pouso Alegre mafic rocks cannot be used to extend the UHP belt of the West Gondwana orogen to the Southern Brasília orogen. Nevertheless, the clinopyroxene-garnet amphibolite could be related to a relatively high P metamorphism in the root of the Ediacaran continent-continent collisional zone that may link those orogens.

The calculated low maximal exhumation rate of 1 mm y^{-1} for the clinopyroxene-garnet amphibolite, and high geothermal gradient for

Table 2
Correlations between the main occurrences of retro-eclogites from the Southern Brasília orogen. Data from: 1) This study; 2) Coelho et al. (2017); 3) Campos Neto et al. (2011); 4) Reno et al. (2009); 5) Campos Neto and Caby (1999); 6) Trouw (2008); 7) Hoppe et al. (1985); 8) Luvizotto (2003); 9) Hoppe et al. (1989); 10) Garcia and Campos Neto (2003); 11) Campos Neto and Caby (2000).

	Pouso Alegre	Liberdade nappe	Varginha nappe	São Sebastião do Paraíso	Carmo da Cachoeira
Protolith age (Ma)	1520[1]; 1504 ± 29[2]	–	1400[6]	_	_
Method	SIMS and LA-ICP-MS[1]; SHRIMP[2]	–	SHRIMP[6]	_	_
Lithochemical signature	N-MORB to T-MORB[1]	N-MORB[3]	_	Tholeiite signature[7]	_
Isotopic signature	_	Sm-Nd t_{DM} ages 1.15–1.48 Ga epsilon $Nd_{(610)}$: (−3 to +0.2)[3]	_	_	_
Interpretation	intrusion (dyke)[1]; paleodykes[2]	oceanic crust [3]	_	_	_
Metamorphism age	600–630[1]; 623 ± 16 (n = 9)[2]	699 ± 25 (n = 5)[3]; 678 ± 29 (n = 4)[4]; 600–630[2]	670; 620[6]	_	_
Method	SIMS and LA-ICP-MS[1]; SHRIMP[2]	SHRIMP[3]; HR-SIMS[4]; SHRIMP[2]	SHRIMP[6]	_	_
Interpretation	Decompression[1]; eclogitization at minimum pressure[2]	HP metamorphism[3]; eclogitization at minimum pressures of 17 kbar[2]; eclogitization[4]	pre-collisional metamorphism; collisional metamorphism[6]	_	_
Evidence for interpretation	Cpx and Cam inclusion in Zrn rim and 2 patterns for REE[1]; absence of Eu anomaly in REE in the rims[2]	_	_	_	_
Peak P-T constraints	720 ± 30 °C at 14 ± 2 kbar[1]; 692 ± 60 °C at 12.7 ± 2.7 kbar [2]	660 °C at 17.5 kbar[5]	eclogite facies[6]	711–799 °C at 12.5–13.5 kbar[8]; 650–700 °C at 12–14 kbar[9]	Cpx(Jd0.20)–Grt–Pl 818 °C at 18.5 kbar[10]
Evidence	P-T modeling (mineral integration, mineral inclusions in Rt and Zrn and Zr-in-rutile thermometry)[1]; avPT with THERMOCALC[2]	lamella in Cpx with XJd up to 0.76 included in Grt[5]	assemblage Cpx + Grt, with Pl overgrowth around garnet indicating decompression[6]	Grt-Cpx thermomether[8], Xjad in Cpx baromether[9]	Cpx bearing assemblage. TWEEQU equilibria and Jd content 0.20[10]
Retrogression P-T constraints	550–700 °C at <7 kbar[1]; 598 ± 58 °C at 5.5 ± 1.1 kbar[2]	650 ± 75 °C at 11.6 kbar[5]	granulite facies[6]	490 ± 50 °C[8]	Amp–Grt–Pl 665 °C at 10.8 Kbar[10]
Evidence	trace elements in Zrn and inclusions in Zrn rim[1]; considering garnet rim composition[2]	garnet-amphibole thermometry in the corona[5]	Opx indicatory[6]	Hbl + Pl in symplectites around Grt[8]	amphibole bearing assemblage[10]
Host rocks	Paleoproterozoic basement and migmatitic Sil-Grt gneiss[1]; Bt gneiss from the basement[2]	biotite gneisses and feldspathic schists with intercalations of muscovite schist and quartzite. (Liberdade Nappe units)	Ky-Kfs gneiss[6]	garnet-bearing biotite gneiss (upper Araxá Group)[9]	Ky- and Grt-bearing schists, gneisses and quartzites[10]; active margin metasediments[11]
Host rock age protolith	2100[1], 800[2] Ma	_	_	_	_
Age method	LA-ICPC-MS[1]	_	_	_	_
Host rock age metamorphism	626 ± 5 Ma and 632 ± 2 Ma, 672 ± 4(Zrn) Ma and 634 ± 3 Ma (Mnz)[1]	_	_	_	_
Age method	LA-ICPC-MS and SIMS for Mnz[1]	_	_	_	_
P-T constraints	750 °C at 13 kbar[1]	_	_	_	Metapelite: muscovite- (473 °C at 5.3 kbar) and biotite- (521 °C at 5.5 kbar) bearing mineral associations[10]
P-T method	avPT THERIAK-DOMINO[1]	_	_	_	TWEEQU equilibria[10]

the symplectite and corona formation stage would indicate that exhumation was tectonic-driven.

The present study highlights the need for detailed investigations on other rocks with similar compositions and textures that have been called "retro-eclogites" in the Southern Brasília orogen (Table 2), as they possibly do not record the required PT conditions to be formed during an ocean subduction process.

Supplementary data to this article can be found online at https://doi.org/10.1016/j.lithos.2017.09.025.

Acknowledgments

This research was supported by the Brazilian "Science Without Borders Program" with a scholarship and grant to M. Tedeschi (CNPq 202054/2015-2), and CODEMIG and CNPq projects coordinated by A. Pedrosa Soares. We are grateful to all those institutions. We also thank T. Pettke and A. Berger, University of Bern, for analytical assistance with the LA-ICP-MS and SEM, and L. Garcia and M. Flores for assistance with EPMA analysis in Federal University of Minas Gerais (LMA-UFMG). A. Pedrosa Soares and I. Dussin are grateful to the CNPq for their productivity grants. We thank R. Moraes and an anonymous reviewer for their fruitful comments and suggestions and M. Scambelluri for his efficient editorial handling.

Appendix A. Analytical methods

A.1. Sample preparation, imaging and qualitative analyses

Zircon, rutile and monazite were separated, using standard rock crushing and heavy mineral separation techniques. Grains were individually selected, picked and mounted in epoxy resin. Grain mounts were polished to expose the grain centres. Backscatter electron images (BSE) for monazite and rutile were performed with a ZEISS EVO50 scanning electron microscope (SEM) at the Institute of Geological Sciences (University of Bern). Zircons were imaged in cathodoluminescence (CL) to domain identification using a Quanta-250-FEI SEM fitted with a CL detector at the Multilab from Universidade do Estado do Rio de Janeiro (UERJ). Mineral abbreviations follow Whitney and Evans (2010).

A.2. Bulk rock analysis

Major and trace elements of four samples (MT-13, MT-17, MT-19 and MT-20) were analyzed at the SGS GEOSOL laboratories (Brazil). Major element oxides were determined using X-ray Fluorescence and trace elements by ICP-MS. Results are reported in Supplementary Data 1. Due to extensive weathering, sample MT-22A from the migmatitic Sil-Grt gneiss was not analyzed for bulk-rock chemistry.

A.3. Electron probe micro-analysis

The Cpx-Grt amphibolite (MT-13) was analyzed by electron probe micro-analyser (EPMA) using both quantitative spot analyses and X-ray compositional mapping in wavelength-dispersive mode. EPMA analyses were carried out with a JEOL JXA-8200 superprobe at the Institute of Geological Sciences (University of Bern). Operating conditions for spot analyses were 15 keV accelerating voltage, 10 nA beam current and 40 s dwell times (including 2 × 10 s of background measurement). Mineral inclusions in zircon and rutile were analyzed with spots of 1 μm and 3 μm. The following standards were used: almandine (Si, Fe, Al), forsterite (Mg), orthoclase (K), anorthite (Ca), albite (Na), tephrite (Mn) and ilmenite (Ti) for garnet, and wollastonite (Si), orthoclase (K), anorthite (Al, Ca), albite (Na), forsterite (Mg), almandine (Fe), tephrite (Mn) and ilmenite (Ti) for pyroxene and amphibole. Compositional maps were acquired following the procedure described in Lanari et al. (2012, 2013) using 15 KeV accelerating voltage, 100 nA beam current and dwell times of 200 ms. A map of 655,500 pixels over an area of 950 × 690 μm^2 with a step size of 1 μm was acquired on sample MT-13 (Fig. 3) and two maps of 324,000 and 422,500 pixels over areas of 600 × 540 μm^2 and 650 × 650 μm^2 with a step size of 3 μm were acquired on sample MT-22A (Supplementary Fig. S.6). Point analyses were also measured on the same area to be used as internal standards (De Andrade et al., 2006).

The compositional maps were classified and converted into concentration maps of oxide weight percentage using the software XMapTools 2.3.1 (Lanari et al., 2014). Local bulk compositions were approximated from merged oxide weight percentage maps using the export built-in function of XMapTools by integrating the pixel compositions of specific domains after a density correction (Mészaros et al., 2016; Lanari and Engi, 2017). The density of each phase was estimated using Theriak (de Capitani and Brown, 1987) at 700 °C and 12 kbar. This technique to obtain local bulk composition was applied to the different retrogressed domains such as the symplectite and corona areas (Fig. 3e).

The migmatitic Grt-Amp gneiss (MT-17) and the migmatitic Sil-Grt gneiss (MT-22A) single spot analyses were performed with a JEOL JXA-8900RL electron microprobe of the Microanalysis Laboratory of Federal University of Minas Gerais (Brazil). The operating conditions were: 15 kV acceleration voltages, 5 μm beam diameter and 20 nA beam current. Standards used were quartz (Si), Al_2O_3 (Al), jadeite (Na), periclase (Mg), sanidine (K), almandine (Fe), anortite (Ca), rutile (Ti) and rodonite (Mn).

A.4. Trace elements LA-ICP-MS

Trace elements compositions were obtained using a GeoLas-Pro 193 nm ArF Excimer laser ablation system (Lambda Physik, Germany) combined with an Elan DRC-e quadrupole mass spectrometer (Perkin Elmer, Canada) at the Institute of Geological Sciences (University of Bern). Conditions for laser fluency, frequency and spot size were 6 J/cm^{-2}, 6 Hz and 24 μm and 32 μm for zircon (MT-13); 6 J/cm^{-2}, 8 Hz and 32, 44, 60 and 90 μm for rutile (MT-13); 6 J/cm^{-2}, 6 Hz and 24 μm for monazite (MT-22A) and 8 J/cm^{-2}, 10 Hz and 90 μm for garnet (MT-13 and MT-22A). Both the acquisition and reduction data were performed in blocks of 1 h using NIST SRM 612 as primary standard and USGS GSD-1G as secondary reference material. The measurement accuracy is generally within 0.7–3% (1σ, N = 6). The software SILLS 132 (Guillong et al., 2008) was used for data reduction. The internal standard values were: TiO_2 = 99 wt% for rutile; SiO_2 = 32.45 wt% for zircon; P_2O_5 = 29.55 wt% for monazite and SiO_2 = 39 wt% (MT-13) and 37 wt% (MT-22A) for garnet. For zircon and monazite spots were placed near or at the same position of the U-Pb dating spots and in the same CL-domains. Results are reported in Supplementary Data 2 for MT13 and Supplementary Data 3 for MT22A.

A.5. Accessory mineral thermometry

Zr-in-rutile and Ti-in-zircon temperatures for the Cpx-Grt amphibolite (MT-13) were estimated using the calibrations of Tomkins et al. (2007) for α-quartz and Watson et al. (2006). The uncertainty for the obtained temperatures in rutile was calculated following the procedure of Ewing et al. (2013), by summing in quadrature an estimate of the relative errors contributed to the calculated temperature (in Kelvin) by the pressure estimate (±2 kbar), the analytical uncertainty on the measurement of Zr (2.2% based on secondary standard GSD-1G), and the uncertainty inherent in the calibration. An uncertainty of ±3% on the calibration of Watson et al. (2006) is assumed, since Tomkins et al. (2007) do not detail the uncertainty from the calibration and the results from both calibrations are inside the uncertainty above. The propagated overall uncertainty is ±4%. For Ti-thermometry the uncertainty on Ti LA-ICP-MS measurement was estimated to 2.5%, the uncertainty from the Watson et al. (2006) equation is <1%, supplying a propagated uncertainty of ±2.6%.

A.6. LA-ICP-MS U-Pb zircon dating

U-Pb isotopic analyses were performed with several LA-ICP-MS systems: (1) for samples MT-17, MT-19 and MT-20 using a microprobe ArF Excimer Laser 193 μm da Photon (Machines Inc. Model ATLEX SI) coupled to the high resolution Neptune-Plus multicollector (Thermo Fisher Scientific, USA), at the MULTILAB, Universidade do Estado do Rio de Janeiro (UERJ). Instrument set up parameters were 8–9 mJ/cm^2 laser fluency, 10 Hz, 25 μm and Laser energy spot between 20 and 40 %. U-Pb data were standardized using GJ-1 zircon (reference 609 Ma, Jackson et al., 2004) as primary standard and tested using the zircon 91,500 (reference 1065 Ma, Wiedenbeck et al., 1995) as secondary standard. External errors were calculated with the error propagation of individual measurements of GJ-1 and the individual measurements of each spot. Data reduction was done using an Excel program developed by Chemale et al. (2012). (2) Sample MT-13, was analyzed with a Thermo-Finnigan Neptune multicollector ICP-MS (Thermo-Finnigan Neptune multicollector) coupled to a Photon-Machines 193 nm G2 laser system at Universidade Federal de Ouro Preto (UFOP) following the procedure described in Santos et al. (2017). Instrument set up parameters were a spot size of 20 μm, a frequency of 6 Hz, 10% energy, and an intensity of 0.3 mJ. U-Pb data were standardized using the zircon GJ-1 (reference 609 Ma, Jackson et al., 2004) as primary standard and tested using the zircon Pleisovice (reference 337 Ma, Slama et al., 2008) as secondary standard. External errors were propagated considering the internal reproducibility of the individual ratios, external reproducibility of GJ-1, long-term uncertainty of the validation material, the ratio uncertainties of the reference material and Pb-common ratio uncertainty (Santos et al., 2017). Data evaluation for each spot was filtered considering outliers values of common Pb contents, errors of isotopic ratios and high percentages of discordance and Th/U ratios. From the selected spots, only those with discordance lesser than 10% were used to age calculations and plotted in Concordia diagrams. The Concordia diagram and histograms were obtained using the software Isoplot/Ex (Ludwig, 2003) and Density Plotter for sample MT-13 (Vermeesch, 2012). Individual uncertainties are quoted at 1σ level. The confidence level for weighted average is 95%. The results from U-Pb LA-ICP-MS analyses are available in the Supplementary Data 2 for MT-13, 3 for MT-22A, 4 for MT-17, 5 for MT-19 and 6 for MT-20.

A.7. SIMS U-Th-Pb dating

U-Th-Pb geochronology of zircon from the Cpx-Grt amphibolite MT-13 and monazite from the migmatitic Sil-Grt gneiss MT-22A were carried out using the SwissSIMS Cameca IMS 1280-HR (University of Lausanne). Basic instrument set up parameters (ca. 3–5 nA, 25 μm O_2^- primary beam, mass resolution M/ΔM ~5000, energy window 40 eV) are similar to those previously described for zircon U-Th-Pb analysis by Whitehouse and Kamber (2005). The mono-collection peak-hopping routine used an automatic routine in the Cameca CIPS software to scan over the peaks and choose the peak centre for major peaks or to extrapolate the mass to B-field curve for minor peaks (e.g. ^{204}Pb was calibrated by centring the $^{94}Zr_2^{16}O$ peak, ^{207}Pb and ^{208}Pb by centring the ^{206}Pb peak). Measured peaks include $^{90}Zr_2^{16}O$, $^{94}Zr_2^{16}O$, ^{204}Pb, ^{206}Pb, ^{207}Pb, ^{208}Pb, ^{238}U, $^{232}Th^{16}O$, $^{238}U^{16}O$ and $^{238}U^{16}O_2$ for zircon and $^{140}Ce^{31}P^{16}O_2$, $^{232}Th^{143}Nd^{16}O_2$, $^{141}Pr\ ^{31}P^{16}O_2$, ^{204}Pb, ^{206}Pb, ^{207}Pb, ^{208}Pb, ^{238}U, ^{232}Th, $^{232}Th^{16}O$, $^{238}U^{16}O$ for monazite. U-Pb-Th data were standardized to 91,500 zircon (1065 Ma, Wiedenbeck et al., 1995) and USGS44069 monazite (425 Ma, Aleinikoff et al., 2006). Secondary standards run in the same analytical session reproduced average $^{206}Pb/^{238}U$ ages within reference values: TEM zircon 418 ± 6 Ma (reference 417 Ma, Black et al., 2003), Pleisovice zircon 340 ± 4 Ma (reference 337 Ma, Slama et al., 2008), Itambé monazite 507 ± 6 Ma (reference 513 Ma, Gonçalves et al., 2016). Uncertainty on standard $^{206}Pb/^{238}U$ – UO_2/U calibration were 1.4% for zircon and 1.13% for monazite, which were propagated to the data as external error. Common Pb correction was based on the measured ^{204}Pb signal (when significant relative to background) assuming the present day model terrestrial Pb composition of Stacey and Kramers (1975). Radiogenic ratios and single ages were calculated using the CIPS program compiled by Martin Whitehouse. Age calculations use the decay constant recommendations of Steiger and Jäger (1977). The program IsoPlot Ex 4.15 (Ludwig, 2003) was employed to plot the diagrams and calculate concordia and weighted average ages. Individual uncertainties are quoted at 1σ level and the confidence level for weighted average is 95%. Uncertainty on average $^{206}Pb/^{238}U$ ages is forced to be no less than the reproducibility of the standard on the same analytical session. The results from U-Pb SIMS analyses are available in the Supplementary Data 2 MT-13 and 3 for MT-22A.

References

Aleinikoff, J.N., Schenck, W.S., Plank, M.O., Srogi, L., Fanning, C.M., Kamo, S.L., Bosbyshell, H., 2006. Deciphering igneous and metamorphic events in high-grade rocks of the Wilmington Complex, Delaware: morphology, cathodoluminescence and backscattered electron zoning and SHRIMP U–Pb geochronology of zircon and monazite. Geol. Soc. Am. Bull. 118, 39–64.

Baldwin, J.A., Powell, R., Brown, M., Moraes, R., Fuck, R.A., 2005. Modeling of mineral equilibria in ultrahigh-temperature metamorphic rocks from the Anápolis-Itauçu Complex, central Brazil. Journal of Metamorphic Geology 23, 511–531.

Belém, J., Pedrosa-Soares, A.C., Noce, C.M., da Silva, L.C., Armstrong, R., Fleck, A., Gradim, C.T., Queiroga, G.N., 2011. Precusor basin versus orogenic basins: examples from the Andrelândia Group basend on zircon U-Pb (LA-ICP-MS) and lithochemical analysis. Geonomos 19, 224–243.

Black, L.P., Kamo, S.L., Allen, C.M., Aleinikoff, J.N., Davis, D.W., Korsch, R.J., Foudoulis, C., 2003. TEMORA 1: a new zircon standard for Phanerozoic U-Pb geochronology. Chem. Geol. 200, 155–170.

Brouwer, F.M., Engi, M., 2005. Staurolite and other high-alumina phases in Alpine eclogite: analysis of domain evolution. Canadian Mineralogist 43, 105–128.

Brown, M., 2007. Metamorphic conditions in orogenic belts: a record of secular change. International Geology Review 49, 193–234.

Brown, M., 2009. Metamorphic patterns in orogenic systems and the geological record. Geological Society, London, Special Publications 318, 37–74.

Bucher, K., Frey, M., 2002. Petrogenesis of Metamorphic Rocks. seventh ed. Springer, Berlim.

Burbank, D.W., 2002. Rates of erosion and their implications for exhumation. Mineralogical Magazine 66, 25–52.

Caddick, M.J., Konopasek, J., Thompson, A.B., 2010. Preservation of garnet growth zoning and the duration of prograde metamorphism. Journal of Petrology 51, 2327–2347.

Campos Neto, M.C., Caby, R., 1999. Neoproterozoic high-pressure metamorphism and tectonic constraint from the nappe system south of the Sao Francisco Craton, southeast Brazil. Precambrian Research 97 (1–2), 3–26.

Campos Neto, M.C., Caby, R., 2000. Lower crust extrusion and terrane accretion in the Neoproterozoic nappes of southeast Brazil: petrologic and structural constraints. Tectonics 19 (4), 669–687.

Campos Neto, M.D.C., Basei, M.A.S., Assis Janasi, V.D., Moraes, R., 2011. Orogen migration and tectonic setting of the Andrelândia Nappe system: an Ediacaran western Gondwana collage, south of São Francisco craton. Journal of South American Earth Sciences 32, 393–406.

Carlson, W.D., Johnson, C.D., 1991. Coronal reaction textures in garnet amphibolites of the Llano Uplift. American Mineralogist 76, 756–772.

Centrella, S., Austrheim, H., Putnis, A., 2015. Coupled mass transfer through a fluid phase and volume preservation during the hydration of granulite: an example from the Bergen Arcs, Norway. Lithos 236-237:245–255. https://doi.org/10.1016/j.lithos.2015.09.010.

Chakraborty, S., Mukhopadhyay, D., Chowdhury, P., Rubatto, D., Anczkiewicz, R., Trepmann, C., Gaidies, F., Sorcar, N., Dasgupta, S., 2017. Channel flow and localized fault bounded slice tectonics (LFBST): insights from petrological, structural, geochronological and geospeedometric studies in the Sikkim Himalaya, NE India. Lithos 282–283, 464–482.

Chemale, F., Kawashita, K., Dussin, I.A., Avila, J.N., Justino, D., Bertotti, A., 2012. U-Pb zircon in situ dating with LA-MC-ICP-MS using a mixed detector configuration. An. Acad. Bras. Cienc. 84, 275–295.

Choudhuri, A., Fiori, A.P., Winters, A.A.M., Bettencourt, J.S., Rodrigues, J.E., 1978. A note on small bodies of eclogite as inclusions in high grade gneisses north of Pouso Alegre, Minas Gerais. Revista Brasileira de Geociencias 8, 63–68.

Cioffi, C.R., Campos Neto, M.D.C., Möller, A., Rocha, B.C., 2016. Paleoproterozoic continental crust generation events at 2.15 and 2.08 Ga in the basement of the southern Brasília Orogen, SE Brazil. Precambrian Research 275, 176–196.

Cioffi, C.R., Campos Neto, M.D.C., Rocha, B.C.D., Moraes, R., Henrique-Pinto, R., 2012. Geochemical signatures of metasedimentary rocks of high-pressure granulite facies and their relation with partial melting: Carvalhos Klippe, Southern Brasília Belt, Brazil. Journal of South American Earth Sciences 40, 63–76.

Coelho, M.B., Trouw, R.A.J., Ganade, C.E., Vinagre, R., Mendes, J.C., Sato, K., 2017. Constraining timing and P-T conditions of continental collision and late overprinting in the southern Brasília Orogen (SE-Brazil): U-Pb zircon ages and geothermobarometry of the Andrelândia Nappe system. Precambrian Research 292, 194–215.

Cordani, U.G., Brito-Neves, B.B., D'Agrella-Filho, M.S., 2003. From Rodinia to Gondwana: a review of the available evidence from South America. Gondwana Research 6 (2), 275–283.
Corfu, F., Hanchar, J.M., Hoskin, P.W.O., Kinny, P., 2003. Atlas of zircon textures. In: Hanchar, J.M., Hoskin, P.W.O. (Eds.), Zircon. Reviews in Mineralogy and Geochemistry, Washington. 53, pp. 469–500.
Dale, J., Holland, T., Powell, R., 2000. Hornblende-garnet-plagioclase ther-mobarometry: a natural assemblage calibration of the thermodynamics of hornblende. Contributions to Mineralogy and Petrology 140:353–362. https://doi.org/10.1007/s004100000187.
De Andrade, V., Vidal, O., Lewin, E., O'Brien, P., Agard, P., 2006. Quantification of electron microprobe compositional maps of rock thin sections: an optimized method and examples. Journal of Metamorphic Geology 24:655–668. https://doi.org/10.1111/j.1525-1314.2006.00660.x.
de Capitani, C., Brown, T.H., 1987. The computation of chemical equilibrium in complex systems containing non-ideal solutions. Geochimica et Cosmochimica Acta 51, 2639–2652.
de Capitani, C., Petrakakis, K., 2010. The computation of equilibrium assemblage diagrams with Theriak/Domino software. American Mineralogist 95, 1006–1016.
De Wit, M.J., Brito-Neves, B.B., Trouw, R.A.J., Pankhurst, R.J., 2008. Pre-Cenozoic correlations across the South Atlantic region: the ties that bind. In: Pankhurst, R.J., Trouw, R.A.J., Brito-Neves, B.B., De Wit, M.J. (Eds.), West Gondwana: Pre-Cenozoic Correlations Across the Atlantic Region. Geological Society, London, Special Publications 294, pp. 1–8.
Diener, J.F.A., Powell, R., White, R.W., Holland, T.J.B., 2007. A new thermodynamic model for clino- and orthoamphiboles in the system Na2O–CaO–FeO–MgO–Al2O3–SiO2–H2O–O. Journal of Metamorphic Geology 25:631–656. https://doi.org/10.1111/j.1525-1314.2007.00720.x.
Evans, B.W., Trommsdorff, V., Richter, W., 1979. Petrology of an eclogite-metarodingite suite at Cima di Gagnone, Ticino, Switzerland. American Mineralogist 64, 15–31.
Ewing, T., Hermann, J., Rubatto, D., 2013. The robustness of the Zr-in-rutile and Ti-in-zircon thermometers during high-temperature metamorphism (Ivrea-Verbano Zone, northern Italy). Contrib. Mineral. Petrol. 165, 757–779.
Fuck, R., Pimentel, M., Alvarenga, C., Dantas, E., 2017. The Northern Brasília Belt. In: Helibron, M., Cordani, U.G., Alkmim, F.F. (Eds.), São Francisco Craton, Eastern Brazil. Springer International Publishing, Switzerland. https://doi.org/10.1007/978-3-319-01715-0_11 (326 pp.).
Ganade de Araujo, C.E., 2014. Evolução Tectônica da Margem ativa Neoproterozóica do Orógeno Gondwana Oeste na Província Borborema (NE-Brasil). (PhD Thesis). Universidade de São Paulo, p. 243.
Ganade de Araujo, C.E., Rubatto, D., Hermann, J., Cordani, U.G., Caby, R., Basei, M.A., 2014. Ediacaran 2,500-km-long synchronous deep continental subduction in the West Gondwana Orogen. Nature Communications 5:5198. https://doi.org/10.1038/ncomms6198.
Garcia, M.G.M., Campos Neto, M.C., 2003. Contrasting metamorphic conditions in the Neoproterozoic collision-related Nappes south of Sao Francisco Craton, SE Brazil. Journal of South American Earth Sciences 15 (8), 853–870.
Gilotti, J.A., 2013. The realm of ultrahigh-pressure metamorphism. Elements 9 (4), 255–260.
Godard, G., 2001. Eclogites and their geodynamic interpretations: a history. Journal of Geodynamics. Special Issue on the History of Geodynamics 32, 165–203.
Gonçalves, G., Lana, C., Scholz, R., Buick, I.S., Gerdes, A., Kamo, S.L., Corfu, F., Marinho, M.M., Chaves, A., Valeriano, C., Nalini Jr., H.A., 2016. An assessment of monazite from the Itambé pegmatite district for use as U–Pb isotope reference material for microanalysis and implications for the origin of the "Moacyr" monazite. Chem. Geol. 424, 30–50.
Guillong, M., Meier, D.L., Allan, M.M., Heinrich, C.A., Yardley, B.W.D., 2008. SILLS: A MATLAB-based program for the reduction of laser ablation ICP-MS data of homogeneous materials and inclusions. In: Sylvester, P. (Ed.), Laser ablation ICP-MS in the Earth sciences: Current practices and outstanding issues. Mineralogical Association of Canada Short Course Series 40, pp. 328–333.
Guillot, S., Mahéo, G., de Sigoyer, J., Hattori, K., Pêcher, A., 2007. Tethyan and indian subduction viewed from the Himalayan high- to ultra-high pressure meta morphic rocks. Tectonophysics 451, 225–241.
Hart, E., Storey, C., Bruand, E., Schertl, H.-P., Alexander, B.D., 2016. Mineral inclusions in rutile: a novel recorder of HP-UHP metamorphism. Earth and Planetary Science Letters 446, 137–148.
Heilbron, M., Cordani, U., Alkmim, F. (Eds.), 2017. São Francisco Craton, Eastern Brazil. Springer International Publishing, Switzerland. https://doi.org/10.1007/978-3-319-01715-0 (326 pp.).
Heinrich, C.A., 1986. Eclogite facies regional metamorphism of hydrous mafic rocks in the central Alpine Adula Nappe. Journal of Petrology 27 (1), 123–154.
Hermann, J., Rubatto, D., 2003. Relating zircon and monazite domains to garnet growth zones: age and duration of granulite facies metamorphism in the Val Malenco lower crust. Journal of Metamorphic Geology 21, 833–852.
Hermann, J., Rubatto, D., Korsakov, A., Shatsky, V.S., 2001. Multiple zircon growth during fast exhumation of diamondiferous, deeply subducted continental crust (Kokchetav massif, Kazakhstan). Contributions to Mineralogy and Petrology 141, 66–82.
Holland, T., Blundy, J., 1994. Non-ideal interactions in calcic amphiboles and their bearing on amphibole-plagioclase thermometry. Contributions to Mineralogy and Petrology 116:433–447. https://doi.org/10.1007/BF00310910.
Holland, T.J.B., 1990. Activities of components in omphacitic solid solutions. Contributions to Mineralogy and Petrology 105:446–453. https://doi.org/10.1007/BF00286831.
Holland, T.J.B., Powell, R., 1996. Thermodynamics of order-disorder in minerals: I. Symmetric formalism applied to minerals of fixed composition. American Mineralogist 81, 1413–1424.
Holland, T.J.B., Powell, R., 1998. An internally-consistent thermodynamic dataset for phases of petrological interest. Journal of Metamorphic Geology 16, 309–344.
Holland, T.J.B., Powell, R., 2003. Activity-composition relations for phases in petrological calculations: an asymmetric multicomponent formulation. Contributions to Mineralogy and Petrology 145, 492–501.
Hoppe, A., Choudhuri, A., Klein, H., Schmidt, W., 1989. Precambrian eclogites from Minas Gerais, Brazil. International Geological Congress, Washington, pp. 68–69.
Hoppe, A., Klein, H., Choudhuri, A., Schmidt, W., 1985. Eclogitos pré-cambrianos no sudoeste de Minas Gerais. Simpósio de Geologia de Minas Gerais. SBG/Núcleo Minas Gerais, Belo Horizonte, pp. 180–192.
Jackson, S., Pearson, N.J., Griffin, W.L., Belousova, E.A., 2004. The application of laser ablation-inductively coupled plasma-mass spectrometry to in situ U–Pb zircon geochronology. Chem. Geol. 211, 47–69.
Kaczmarek, M.-A., Müntener, O., Rubatto, D., 2008. Trace element chemistry and U–Pb dating of zircons from oceanic gabbros and their relationship with whole rock composition (Lanzo, Italian alps). Contributions to Mineralogy and Petrology 155, 295–312.
Katayama, I., Maruyama, S., 2009. Inclusion study in zircon from ultrahigh-pressure metamorphic rocks in the Kokchetav massif: an excellent tracer of metamorphic history. Journal of the Geological Society 166 (4), 783–796.
Kelly, N., Harley, S., 2005. An integrated microtextural and chemical approach to zircon geochronology: refining the Archean history of the Napier Complex, east Antarctica. Contributions to Mineralogy and Petrology 149, 57–84.
Kohn, M.J., Corrie, S.L., Markley, C., 2015. The fall and rise of metamorphic zircon. American Mineralogist 100, 897–908.
Lanari, P., Engi, M., 2017. Local bulk composition effects on mineral assemblages. In: Kohn, M.J., Lanari, P., Engi, M. (Eds.), Petrochronology. Reviews in Mineralogy and Geochemistry 83, pp. 55–102.
Lanari, P., Giuntoli, F., Loury, C., Burn, M., Engi, M., 2017. An inverse modeling approach to obtain P-T conditions of metamorphic stages involving garnet growth and resorption. European Journal of Mineralogy 29, 181–199.
Lanari, P., Guillot, S., Schwartz, S., Vidal, O., Tricart, P., Riel, N., Beyssac, O., 2012. Diachronous evolution of the alpine continental subduction wedge: evidence from P-T estimates in the Briançonnais Zone houillere (France – Western Alps). Journal of Geodynamics 56-57, 39–54.
Lanari, P., Riel, N., Guillot, S., Vidal, O., Schwartz, S., Pêcher, A., Hattori, K.H., 2013. Deciphering high-pressure metamorphism in collisional context using microprobe mapping methods: application to the Stak eclogitic massif (northwest Himalaya). Geology 41 (2):111–114. https://doi.org/10.1130/g33523.1.
Lanari, P., Vidal, O., De Andrade, V., Dubacq, B., Lewin, E., Grosch, E.G., Schwartz, S., 2014. XMapTools: a MATLAB©-based program for electron microprobe X-ray image processing and geothermobarometry. Computers & Geosciences 62, 227–240.
Liu, F., Zhang, L., Li, X., Slabunov, A.I., Wei, C., Bader, T., 2017. The metamorphic evolution of Paleoproterozoic eclogites in Kuru-Vaara, northern Belomorian Province, Russia: constraints from P-T pseudosections and zircon dating. Precambrian Research 298, 31–47.
Loury, C., Rolland, Y., Cenki-Tok, B., Lanari, P., Guillot, S., 2016. Late Paleozoic evolution of the south Tien Shan: insights from P – T estimates and allanite geochronology on retrogressed eclogites (Chatkal range, Kyrgyzstan). Journal of Geodynamics 96, 62–80.
Ludwig, K.R., 2003. Isoplot Excell version 3.0. A geochronological toolkit for Microsoft Excel. Berkeley Geochronological Centre Special Publication No. 4, Berkeley, California.
Luvizotto, G.L., 2003. Caracterização metamórfica das rochas do grupo Araxá na região de São Sebastião do Paraíso, Sudoeste de Minas Gerais. Universidade Estadual Paulista "Júlio de Mesquita Filho", p. 187.
Mantovani, M.S.M., Brito-Neves, B.B., 2005. The Paranapanema lithospheric block: its importance for Proterozoic (Rodinia, Gondwana) supercontinent theories. Gondwana Research 8 (3), 303–315.
McClelland, W.C., Lapen, T.J., 2013. Linking time to the pressure–temperature path for ultrahigh-pressure rocks. Elements 9, 273–279.
McDonough, W.F., Sun, S.S., 1995. The composition of the earth. Chemical Geology 120, 223–254.
Mészaros, M., Hofmann, B.A., Lanari, P., Korotev, R.L., Gnos, E., Greber, N.D., Greenwood, R.C., Jull, A.J.T., Al-Wagdani, K., Mahjoub, A., Al-Solami, A.A., Habinullah, A.N., 2016. Petrology and geochemistry of feldspathic impact-melt breccia Abar al' Uj 012, the first lunar meteorite from Saudi Arabia. Meteorit. Planet. Sci. 51 (10), 1830–1848.
Motta, R.G., Moraes, R., 2017. Pseudo- and real-inverted metamorphism caused by superposition and extrusion of a stack of nappes: example of the Southern Brasília Orogen, Brazil. International Journal of Earth Sciences. https://doi.org/10.1007/s00531-016-1436-7.
Nasdala, L., Zhang, M., Kempe, U., Panczer, G., Gaft, M., Andrut, M., Plötze, M., 2003. Spectroscopic methods applied to zircon. In: Hanchar, J.M., Hoskin, P.W.O. (Eds.), Zircon. Reviews in Mineralogy and Geochemistry, Washington. 53, pp. 427–467.
Parkinson, C.D., Motoki, A., Onishi, C.T., Maruyama, S., 2001. Ultrahigh-pressure pyrope-kyanite granulites and associated eclogites in Neoproterozoic Nappes of Southeast Brazil. UHPM Workshop. Waseda University, pp. 87–90.
Powell, R., Holland, T.J.B., 2008. On thermobarometry. Journal of Metamorphic Geology 26 (2):155–179. https://doi.org/10.1111/j.1525-1314.2007.00756.x.
Reno, B.L., Brown, M., Kobayashi, K., Nakamura, E., Piccoli, P.M., Trouw, R.A.J., 2009. Eclogite-high-pressure granulite metamorphism records early collision in west Gondwana: new data from the southern Brasilia Belt, Brazil. Journal of the Geological Society 166, 1013–1032.
Ribeiro, A., Nascimento, D., Bongiolo, E., Trouw, R., Polo, H., Tavares, F., Nepomuceno, F., 2011. Geologia da Folha Pouso Alegre 1:100.000. Programa Geologia do Brasil, CPRM-UFRJ, Rio de Janeiro, Brazil.
Robyr, M., Darbellay, B., Baumgartner, L.P., 2014. Matrix-dependent garnet growth in polymetamorphic rocks of the Sesia zone, Italian Alps. Journal of Metamorphic Geology 32 (1):3–24. https://doi.org/10.1111/jmg.12055.

Rocha, B.C., Moraes, R., Möller, A., Cioffi, C.R., Jercinovic, M.J., 2016. Timing of anatexis and melt crystallization in the Socorro-Guaxupé Nappe, SE Brazil: insights from trace element composition of zircon, monazite and garnet coupled to U-Pb geochronology. Lithos 277:337–355. https://doi.org/10.1016/j.lithos.2016.05.020.

Rubatto, D., 2002. Zircon trace element geochemistry: distribution coefficients and the link between U–Pb ages and metamorphism. Chemical Geology 184, 123–138.

Rubatto, D., 2017. Zircon: the metamorphic mineral. In: Kohn, M.J., Lanari, P., Engi, M. (Eds.), Petrochronology. Reviews in Mineralogy and Geochemistry 83, pp. 261–289.

Rubatto, D., Hermann, J., 2001. Exhumation as fast as subduction? Geology 29 (1), 3–6.

Rubatto, D., Hermann, J., Buick, I.S., 2006. Temperature and bulk composition control on the growth of monazite and zircon during low-pressure anatexis (Mount Stafford, central Australia). Journal of Petrology 47, 1973–1996.

Santos, M.M., Lana, C., Scholz, R., Buick, I., Schmitz, M.D., Kamo, S.L., Gerdes, A., Corfu, F., Tapster, S., Lancaster, P., Storey, C.D., Basei, M.A.S., Tohver, E., Alkmim, A., Nalini, H., Krambrock, K., Fantini, C., 2017. A new appraisal of Sri Lankan zircons as reference material for in situ U–Pb geochronology, REE analyses and Lu-Hf isotope tracing. Geostandards Geoanal. Res. J. (in press).

Sawyer, E.W., 2008. The Atlas of migmatites. The Canadian Mineralogist, Special Publication 9. NRC Research Press, Ottawa, p. 371.

Schlunegger, F., Willett, S.D., 1999. Spatial and temporal variations in exhumation of the central Swiss Alps and implications for exhumation mechanisms. In: Ring, U., Brandon, M.T., Lister, G.S., Willett, S.D. (Eds.), Exhumation Processes: Normal Faulting, Ductile Flow and Erosion. Geological Society, London, Special Publications 154, pp. 157–179.

Singh, P., Pant, N.C., Saikia, A., Kundu, A., 2013. The role of amphiboles in the metamorphic evolution of the UHP rocks: a case study from the Tso Morari Complex, northwest Himalayas. International Journal of Earth Sciences (Geologische Rundschau) 102: 2137–2152. https://doi.org/10.1007/s00531-013-0920-6.

Sizova, E., Gerya, T., Brown, M., 2014. Contrasting styles of Phanerozoic and Precambrian continental collision. Gondwana Research 25, 522–545.

Slama, J., Kosler, J., Condon, D.J., Crowley, J.L., Gerdes, A., Hanchar, J.M., Horstwood, M.S.A., Morris, G.A., Nasdala, L., Norberg, N., Schaltegger, U., Schoene, B., Tubrett, M.N., Whitehouse, M.J., 2008. Plesovice zircon - A newnatural reference material for U-Pb and Hf isotopic microanalysis. Chem. Geol. 249, 1–35.

Stacey, J.S., Kramers, J.D., 1975. Approximation of Terrestrial Lead Isotope Evolution by a 2 Stage Model. Earth Planet. Sci. Lett. 26 (2), 207–221.

Steiger, R.H., Jäger, E., 1977. Subcommission on geochronology - Convention on use of decay constants in geochronology and cosmochronology. Earth Planet. Sci. Lett. 36, 359–362.

Tindle, A.G., Webb, P.C., 1994. PROBE-AMPH a spreadsheet program to classify microprobe-derived amphibole analyses. Computers and Geosciences 20, 1201–1228.

Tinkham, D.K., Zuluaga, C.A., Stowell, H.H., 2001. Metapelite phase equilibria modeling in MnNCKFMASH: the effect of variable Al_2O_3 and MgO / (MgO + FeO) on mineral stability. Geological Materials Research 3 (1), 1–42.

Tomkins, H.S., Powell, R., Ellis, D.J., 2007. The pressure dependence of the zirconium-in-rutile thermometer. Journal of Metamorphic Geology 25, 703–713.

Trouw, C.C., 2008. Mapeamento da Folha Virgínia–MG, Geocronologia U-Pb (SHRIMP) em zircões e interpretação geotectônica. (PhD Thesis). Universidade do Rio de Janeiro, p. 127.

Trouw, R.A.J., Heilbron, M., Ribeiro, A., Paciullo, F.V.P., Valeriano, C.M., Almeida, J.C.H., Tupinambá, M., Andreis, R.R., 2000. The central segmento of the Ribeira Belt. In: Cordani, U.G., Milani, E.J., Thomaz Filho, A., Campos, D.A. (Eds.), Tectonic Evolution of South America. 31 International Geological Congress, Rio de Janeiro, pp. 335–365.

Trouw, R.A.J., Peternel, R., Ribeiro, A., Heilbron, M., Vinagre, R., Duffles, P., Trouw, C.C., Fontainha, M., Kussama, H.H., 2013. A new interpretation for the interference zone between the southern Brasília belt and the central Ribeira belt, SE Brazil. Journal of South American Earth Sciences 48, 43–57.

Valeriano, C., 2017. The Southern Brasília Belt. In: Helibron, M., Cordani, U.G., Alkmim, F.F. (Eds.), São Francisco Craton, Eastern Brazil. Springer International Publishing, Switzerland. https://doi.org/10.1007/978-3-319-01715-0_11 (326 pp.).

Vermeesch, P., 2012. On the visualisation of detrital age distributions. Chem. Geol. 312-313, 190–194.

Waters, D., 2003. P-T path from Cpx-Hbl-Pl symplectites. www.earth.ox.ac.uk/~davewa/index.html.

Watson, E.B., Wark, D.A., Thomas, J.B., 2006. Crystallization thermometers for zircon and rutile. Contributions to Mineralogy and Petrology 151, 413–433.

Weller, O.M., St-Onge, M.R., 2017. Record of modern-style plate tectonics in the Palaeoproterozoic Trans-Hudson orogeny. Nature Geoscience 10, 305–311.

Westin, A., Campos Neto, M.C., Hawkesworth, C.J., Cawood, P.A., Dhuime, B., Delavault, H., 2016. A Paleoproterozoic intra-arc basin associated with a juvenile source in the southern Brasilia Orogen: application of U–Pb and Hf–Nd isotopic analyses to provenance studies of complex areas. Precambrian Research 276, 178–193.

White, R.W., Powell, R., Baldwin, J.A., 2008. Calculated phase equilibria involving chemical potentials to investigate the textural evolution of metamorphic rocks. Journal of Metamorphic Geology 26, 181–198.

White, R.W., Powell, R., Clarke, G.L., 2002. The interpretation of reaction textures in Fe-rich metapelitic granulites of the Musgrave block, central Australia: constraints from mineral equilibria calculations in the system K_2O-FeO-MgO-Al_2O_3-SiO_2-H_2O-TiO_2-Fe_2O_3. Journal of Metamorphic Geology 20, 41–55.

White, R.W., Powell, R., Holland, T.J.B., 2007. Progress relating to calculation of partial melting equilibria for metapelites. Journal of Metamorphic Geology 25, 511–527.

Whitehouse, M.J., Kamber, B.S., 2005. Assigning dates to thin gneissic veins in high-grade metamorphic terranes: A cautionary tale from Akilia, southwest Greenland. J. Petrol. 46, 291–318.

Whitehouse, M., Kemp, A.I.S., 2010. On the difficulty of assigning crustal residence, magmatic protolith and metamorphic ages to Lewisian granulites: constraints from combined in situ U–Pb and Lu–Hf isotopes. Geological Society, London, Special Publications 335, 81–101.

Whitney, D.L., Evans, B.W., 2010. Abbreviations for names of rock-forming minerals. Am. Mineral. 95, 185–187.

Wiedenbeck, M., Alle, P., Corfu, F., Griffin, W.L., Meier, M., Oberli, F., Von Quadt, A., Roddick, J.C., Spiegel, W., 1995. 3 natural zircon standards for U-Th-Pb, Lu-Hf, trace-element and REE analyses. Geostandards Newsletter 19, 1–23.

Wilson, M., 1989. Igneous Petrogenesis: A Global Tectonic Approach. first ed. Harper Colins Academic, New York.

Zack, T., Moraes, R., Kronz, A., 2004. Temperature dependence of Zr in rutile: empirical calibration of a rutile thermometer. Contributions to Mineralogy and Petrology 148, 471–488.